NASA/TP–2009-215404

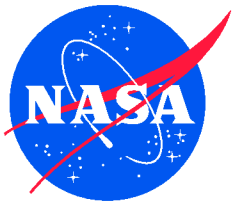

# Influence of Lift Offset on Rotorcraft Performance

*Wayne Johnson*
*Ames Research Center*
*Moffett Field, California*

November 2009

## The NASA STI Program Office . . . in Profile

Since its founding, NASA has been dedicated to the advancement of aeronautics and space science. The NASA Scientific and Technical Information (STI) Program Office plays a key part in helping NASA maintain this important role.

The NASA STI Program Office is operated by Langley Research Center, the Lead Center for NASA's scientific and technical information. The NASA STI Program Office provides access to the NASA STI Database, the largest collection of aeronautical and space science STI in the world. The Program Office is also NASA's institutional mechanism for disseminating the results of its research and development activities. These results are published by NASA in the NASA STI Report Series, which includes the following report types:

- TECHNICAL PUBLICATION. Reports of completed research or a major significant phase of research that present the results of NASA programs and include extensive data or theoretical analysis. Includes compilations of significant scientific and technical data and information deemed to be of continuing reference value. NASA's counterpart of peer-reviewed formal professional papers but has less stringent limitations on manuscript length and extent of graphic presentations.

- TECHNICAL MEMORANDUM. Scientific and technical findings that are preliminary or of specialized interest, e.g., quick release reports, working papers, and bibliographies that contain minimal annotation. Does not contain extensive analysis.

- CONTRACTOR REPORT. Scientific and technical findings by NASA-sponsored contractors and grantees.

- CONFERENCE PUBLICATION. Collected papers from scientific and technical conferences, symposia, seminars, or other meetings sponsored or cosponsored by NASA.

- SPECIAL PUBLICATION. Scientific, technical, or historical information from NASA programs, projects, and missions, often concerned with subjects having substantial public interest.

- TECHNICAL TRANSLATION. English-language translations of foreign scientific and technical material pertinent to NASA's mission.

Specialized services that complement the STI Program Office's diverse offerings include creating custom thesauri, building customized databases, organizing and publishing research results . . . even providing videos.

For more information about the NASA STI Program Office, see the following:

- Access the NASA STI Program Home Page at *http://www.sti.nasa.gov*

- E-mail your question via the Internet to help@sti.nasa.gov

- Fax your question to the NASA Access Help Desk at (301) 621-0134

- Telephone the NASA Access Help Desk at (301) 621-0390

- Write to:
  NASA Access Help Desk
  NASA Center for AeroSpace Information
  7115 Standard Drive
  Hanover, MD 21076-1320

NASA/TP–2009-215404

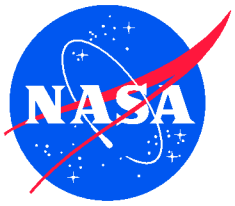

# Influence of Lift Offset on Rotorcraft Performance

*Wayne Johnson*
*Ames Research Center*
*Moffett Field, California*

National Aeronautics and
Space Administration

Ames Research Center
Moffett Field, California 94035-1000

**November 2009**

Available from:

NASA Center for AeroSpace Information
7115 Standard Drive
Hanover, MD 21076-1320
(301) 621-0390

National Technical Information Service
5285 Port Royal Road
Springfield, VA 22161
(703) 487-4650

**TABLE OF CONTENTS**

## LIST OF FIGURES

## LIST OF FIGURES (cont.)



## LIST OF TABLES

## NOMENCLATURE

| | |
|---|---|
| $A$ | disk area (one rotor) |
| $A_b$ | blade area (all rotors) |
| $A_p$ | projected area of twin rotors, $(2–m)A$ |
| $A_r$ | reference area; A for coaxial configuration, and 2A for tandem configuration |
| $c$ | blade chord |
| $c_d$ | mean drag coefficient, $8(C_{Po}/\sigma)/f(\mu)$ |
| $C_T$ | rotor thrust coefficient, $T/(\rho A_r V_{tip}^2)$ |
| $C_T/\sigma$ | thrust coefficient divided by solidity, $T/(\rho A_b V_{tip}^2)$ |
| $C_P$ | power coefficient, $P/(\rho A_r V_{tip}^3)$ |
| $C_P/\sigma$ | power coefficient divided by solidity, $P/(\rho A_b V_{tip}^3)$ |
| $C_W$ | weight coefficient, $W/(\rho A_r V_{tip}^2)$ |
| $C_W/\sigma$ | weight coefficient divided by solidity, $W/(\rho A_b V_{tip}^2)$ |
| $d$ | horizontal separation between rotor hubs (lateral or longitudinal) |
| $D$ | rotor diameter, $2R$ |
| $D/q$ | airframe drag divided by dynamic pressure |
| $f(\mu)$ | factor in profile power accounting for increase of rotor-blade mean dynamic pressure with advance ratio |
| $FM$ | rotor-hover figure of merit, $\left(T\sqrt{T/2\rho A_p}\right)/P$ |
| $L/D$ | aircraft effective lift-to-drag ratio, $WV/P$ (based on cruise power) |
| $L/D_e$ | rotor effective lift-to-drag ratio, $TV/(P_i+P_o)$ (based on rotor induced and profile power) |
| $m$ | overlap ratio of twin rotors |
| $M_{at}$ | advancing tip Mach number |
| $\Delta M_x/LR$ | lift offset (differential rotor roll moment, as a fraction of rotor lift times radius) |
| $N$ | number of blades |
| $P$ | aircraft power |
| $P_\ell$ | lower-rotor power |
| $P_{ref}$ | reference power, $T\sqrt{T/2\rho A_p}$ and $T^2/(2\rho AV)$ in cruise |
| $P_u$ | upper-rotor power |
| $P_i$ | induced power |
| $P_o$ | profile power |
| $P_{ref}$ | reference power |
| $r$ | blade radius |
| $R$ | rotor radius |
| $t/c$ | blade thickness-to-chord ratio |
| $T$ | rotor thrust |
| $T_\ell$ | lower-rotor thrust |
| $T_u$ | upper-rotor thrust |
| $V$ | flight speed |
| $V_{tip}$ | rotor tip speed |
| $W$ | gross weight |
| $W/A$ | disk loading |
| $W/S$ | wing loading |
| $y$ | rotor disk lateral coordinate |
| $z$ | vertical separation between rotors |
| $\eta$ | propeller efficiency, $TV/P$ |
| $\mu$ | advance ratio, $V/V_{tip}$ |
| $\rho$ | air density |
| $\sigma$ | rotor solidity, $Nc/\pi R$ |
| RGW | referred gross weight |
| ISA | International Standard Atmosphere |
| SLS | Sea Level Standard |

# INFLUENCE OF LIFT OFFSET ON ROTORCRAFT PERFORMANCE

Wayne Johnson

Ames Research Center

## ABSTRACT

The influence of lift offset on the performance of several rotorcraft configurations is explored. A lift-offset rotor, or advancing blade concept, is a hingeless rotor that can attain good efficiency at high speed by operating with more lift on the advancing side than on the retreating side of the rotor disk. The calculated performance capability of modern-technology coaxial rotors utilizing a lift offset is examined, including rotor performance optimized for hover and high-speed cruise. The ideal induced power loss of coaxial rotors in hover and twin rotors in forward flight is presented. The aerodynamic modeling requirements for performance calculations are evaluated, including wake and drag models for the high-speed flight condition. The influence of configuration on the performance of rotorcraft with lift-offset rotors is explored, considering tandem and side-by-side rotorcraft as well as wing-rotor lift share.

## INTRODUCTION

By operating a rotor in edgewise flight with lift offset—more lift on the advancing side than on the retreating side of the rotor disk—it is possible to attain good performance at high forward speed. A conventional rotor with an articulated hub is constrained to operate with small hub moments. In forward flight, the retreating side of the disk is not able to generate much lift because of low dynamic pressure and stall, so for roll-moment balance the advancing side is not allowed to generate much lift either. The resulting load distribution over the rotor disk is far from optimum for either induced or profile power losses, and the rotor efficiency and lift capability steadily decrease with forward speed. Even hingeless and bearingless rotors are generally not designed for the blades and hubs to carry significant roll moment, and thus they encounter similar aerodynamic performance limitations. However, a very stiff hingeless rotor can be designed that will permit operation with significant roll moment, say rotor-lift offsets of 20%. Roll-moment balance of the entire aircraft requires either twin main rotors or perhaps a wing. The coaxial helicopter configuration with lift-offset rotors is known as the Advancing Blade Concept (ABC).

The lift-offset concept was demonstrated for the coaxial configuration (ABC) by the XH-59A flight demonstration program of the 1970s (ref. 1). While confirming the basic viability of the concept, the aerodynamic performance of the XH-59A was compromised by the choice of airfoils, planform, and twist, as well as by high hub drag. In addition, the stiff hingeless rotors led to a heavy hub design and high vibration in flight. Recent interest in high-speed, heavy-lift rotorcraft makes it appropriate to reexamine the capability of lift-offset rotors, including the impact of current and advanced technology. The NASA Heavy Lift Rotorcraft Systems Investigation (ref. 2) considered the Large Advancing Blade Concept (LABC) as one of the three configurations designed and analyzed. Sikorsky Aircraft is exploring the ABC in the context of modern technology, including the X2 flight demonstrator (ref. 3). Interest has also been expressed in the possible application of lift-offset rotors to other twin-rotor configurations.

This paper has three objectives: First, the calculated performance capability of modern-technology coaxial rotors utilizing lift offset is examined, including rotor performance optimized for hover and high-speed cruise. Second, the aerodynamic modeling requirements for performance calculations are established, including wake and drag models for the high-speed flight condition. Third, the influence of configuration on the performance of rotorcraft with lift-offset rotors is explored, considering tandem and side-by-side configurations as well as wing-rotor lift share. The aircraft performance was calculated using the comprehensive analysis CAMRAD II. As foundation for these results, performance metrics are discussed, and comparisons are presented of calculated and measured performance of coaxial and tandem rotorcraft.

## BASELINE COAXIAL CONFIGURATION

The baseline configuration is a coaxial rotorcraft utilizing lift-offset rotors, summarized in table 1 and illustrated in figure 1. The aircraft definition is not the product of a conceptual design analysis, but rather was developed from basic system parameters. A heavy-lift transport is considered, so a gross weight of 150,000 lb is used. One conclusion of the NASA Heavy Lift Rotorcraft Systems Investigation (ref. 2) was that the lift-offset rotor is best suited for cruise at moderate speeds and altitude. Thus the design conditions here are takeoff (hover) at atmospheric conditions of 5k/ISA+20°C, and cruise at 250 knots and 5k/ISA+20°C. Based on reference 2 and subsequent studies, it is appropriate to design to a disk loading $W/A$ = 15 lb/ft$^2$ and cruise blade loading $C_T/\sigma$ = 0.10 (thrust-weighted). Thus the rotor disk area is 10,000 ft$^2$ (one rotor), and the rotor diameter 112.8 ft. The vertical separation of the rotors is $z/D$ = 0.06 for the baseline.

At 250 knots, auxiliary propulsion (preferably propellers) is required. A small wing is used to mount the propellers, and also unload the rotor in cruise (thereby reducing the required rotor solidity). The rotor cruise thrust is $T/W$ = 0.8 for the baseline, with a wing loading of 120 lb/ft$^2$. The result is a wing area of 250 ft$^2$, and an aspect ratio of 6 gives the wing span 38.7 ft.

Advanced airfoils are assumed, permitting an advancing tip Mach number of $M_{at}$ = 0.90, which is about 5% greater than the optimum found using airfoils on current rotorcraft. It is also assumed that for the thick root sections of this hingeless rotor, airfoils can be designed with drag and maximum lift similar to current 10–11% thick rotor airfoils. A blade structural design (which has not been done for this rotor) will define the required root thickness, for which the airfoils must be designed. The design criterion will be the thickness-to-radius ratio, so the inverse taper of the present blade design implies a larger thickness-to-chord ratio than for a tapered blade.

From the flight speed of 250 knots and $M_{at}$ = 0.90, it follows that cruise tip speed is 600 ft/sec, and the advance ratio is $V/V_{tip}$ = 0.70. Then cruise $C_T/\sigma$ = 0.10 and $T/W$ = 0.8 gives a solidity of $\sigma$ = 0.0871 for each rotor, and $\sigma$ = 0.1742 for both rotors (based on the projected disk area). Four blades per rotor gives a reasonable blade aspect ratio.

A hover tip speed of 700 ft/sec corresponds to a cruise rotor speed reduction of 14%, and results in a hover blade loading of $C_W/\sigma$ = 0.092.

The rotor power, rotor drag, and wing drag are calculated using the comprehensive analysis, including interference between the rotor and wing. To complete the calculation of the aircraft performance, a fuselage and hub drag of $D/q$ = 50.0 ft$^2$ is used, and a propeller propulsive efficiency of $\eta$ = 0.90. The scaled fuselage and hub drag is $D/q/(\mathrm{W}/1000)^{2/3}$ = 1.77. For comparison, typically $D/q/(\mathrm{W}/1000)^{2/3}$ = 1.4 for current turboprop aircraft, and $D/q/(\mathrm{W}/1000)^{2/3}$ = 0.85 for low-drag rotor hubs (ref. 2).

Based on the assumptions for the rotor airfoil characteristics, the propeller propulsive efficiency, and the level of fuselage and hub drag, the calculated aircraft power is probably somewhat optimistic.

## PERFORMANCE METRICS

### Momentum Theory for Coaxial Rotor in Hover

A coaxial rotor has better hover efficiency than the equivalent single rotor (no separation), primarily because of the contraction of the upper-rotor wake before it reaches the lower rotor. Canceling of swirl losses is a small effect for helicopter rotor loadings. For the performance of the aircraft in hover, elimination of the tail-rotor power loss is a substantial benefit of the coaxial configuration. Tip-vortex visualization on a Ka-32 (ref. 4) shows that the far-wake contraction is 85% for the upper rotor and 91% for the lower rotor (for vertical spacing $z/D$ = 0.10), compared to 78% for a single rotor. The upper-rotor contraction when it reaches the lower rotor is 85%.

Consider coaxial rotors with area $A$ of each rotor and total thrust $T = T_u + T_\ell$. Define the reference velocity as $v_h^2 = T/2\rho A$ (based on area of a single rotor). For coaxial rotors with zero vertical spacing (i.e., a single rotor with the same total solidity), the momentum-theory solution for ideal induced power is $P = Tv_h$. For two separate isolated rotors, the solution is $P = 2(T/2)\sqrt{(T/2)/(2\rho A)} = 2^{-1/2}Tv_h = 0.7071Tv_h$.

Momentum theory is used to determine the induced power for coaxial rotors with very large vertical separation. Figure 2 illustrates the flow model at the lower rotor. Then the lower rotor has no effect on the upper rotor, and the momentum-theory solution for the upper rotor is $v_u^2 = T_u/2\rho A$ and $\mathrm{P}_u = \mathrm{T}_u v_u$. The far-wake velocity of the lower rotor $w_u = 2v_u$ is uniform over the cross-section area $A/2$. This far-wake velocity acts on the lower rotor.

Momentum theory for the lower rotor follows the derivation of section 3-2 of reference 5, with the addition of the interference velocity $w_u = 2v_u$ above the rotor. Mass, momentum, and energy conservation then become:

$$\dot{m} = \int v_\ell dA = \int w_\ell dS$$

$$T_\ell = \int \Delta p_\ell dA = \int \rho w_\ell^2 dS - \rho(2v_u)^2 (A/2)$$

$$P_\ell = \int \Delta p_\ell v_\ell dA = \int \tfrac{1}{2}\rho w_\ell^3 dS - \tfrac{1}{2}\rho(2v_u)^3 (A/2)$$

where $S$ is the area in the far wake of the lower rotor. Calculus of variations shows that the solution for minimum power with constrained thrust is $w_\ell$ uniform over the wake. Thus

$$\dot{m} = \int v_\ell dA = w_\ell S$$

$$T_\ell = \int \Delta p_\ell dA = \rho S w_\ell^2 - 2\rho A {v_u}^2$$

$$P_\ell = \int \Delta p_\ell v_\ell dA = \tfrac{1}{2}\rho S w_\ell^3 - 2\rho A {v_u}^3$$

Momentum theory does not give information about the distribution of the induced velocity $v_\ell$ over the rotor disk. Bernoulli's equation can be used to relate the loading on the rotor disk, $\Delta p_\ell = dT_\ell / dA$, to the far-wake velocity $w_\ell$. Bernoulli's equation is applied from far above the rotor (where the pressure equals ambient) to just above the rotor disk, and from just below the rotor disk to far below (where the pressure again equals ambient); and for stream lines starting from within and without the upper-rotor wake (subscripts $I$ and $O$, for inboard and outboard, respectively). The result is

$$\Delta p_{\ell O} = \tfrac{1}{2}\rho w_\ell^2$$

$$\Delta p_{\ell I} = \tfrac{1}{2}\rho w_\ell^2 - 2\rho v_u^2$$

For an isolated rotor (i.e. without the effect of the upper-rotor wake), uniform far-wake velocity $w_\ell$ implies uniform disk loading $\Delta p_\ell$. For coaxial rotors, the loading is significantly different in the inboard and outboard regions, although uniform in each. Roughly the inboard loading is 1/3 the outboard loading for this optimum power solution. Let $\Delta p_\ell = \alpha(T_\ell / A)$, where $T_\ell$ is the lower-rotor thrust; so $\alpha_I A_I + \alpha_O A_O = A$ ($A_I$ and $A_O$ are the inboard and outboard areas at the rotor disk, which can be determined from mass conservation if $v_\ell$ is known). Then $\alpha_I = \alpha_O - v_u^2 / (T_\ell / 2\rho A)$. Define the mean induced velocity $\bar{v}_\ell = \int v_\ell dA$, and a nonuniform loading parameter $\bar{\alpha} = \int \alpha v_\ell dA / (\bar{v}_\ell A)$; so the power can be written $P_\ell = \int \Delta p_\ell v_\ell dA = \bar{\alpha} T_\ell \bar{v}_\ell$. For an isolated rotor, the optimum solution is uniform disk loading, hence $\bar{\alpha} = 1$; in general $\bar{\alpha}$ is the average of the disk loading weighted by the induced velocity, giving $\bar{\alpha} > 1$. With these definitions, the conservation equations are:

$$\dot{m} = \bar{v}_\ell A = w_\ell S$$

$$T_\ell = \rho A \bar{v}_\ell w_\ell - 2\rho A {v_u}^2$$

$$P_\ell = \tfrac{1}{2}\rho A \bar{v}_\ell w_\ell^2 - 2\rho A {v_u}^3$$

using the mass-flux relation in the momentum and energy equations. For an isolated rotor ($v_u = 0$ and $\bar{\alpha} = 1$), $w_\ell$ is easily eliminated and the usual solution for the mean induced velocity obtained. Define the lower-rotor reference velocity by $v_r^2 = T_\ell / 2\rho A$; and recall that $v_u^2 = T_u / 2\rho A$, so $v_h^2 = T / 2\rho A = v_u^2 + v_r^2$. Eliminating $w_\ell$ gives the relation

$$\bar{\alpha} {v_r}^2 \bar{v}_\ell^2 + {v_u}^3 \bar{v}_\ell = ({v_u}^2 + {v_r}^2)^2$$

Write $v_r = r v_u$, $T_\ell = r^2 T_u = \tau T_u$, and $\bar{v}_\ell = s v_u$. Then the solution of

$$\bar{\alpha}\varpi^2 + s = (1+\tau)^2$$

gives the total power $P = T_u v_u + \bar{\alpha} T_\ell \bar{v}_\ell = (1 + \bar{\alpha}\varpi) T_u v_u$, or

$$P = (1+\tau)^{-3/2} (1 + \bar{\alpha}\varpi) T v_h$$

Given $\tau$, the ratio of the lower and upper induced velocities is

$$s = \frac{1}{2\bar{\alpha}\tau}\left(\sqrt{1 + 4(1+\tau)^2 \bar{\alpha}\tau} - 1\right)$$

Note the thrust and power ratios are then $T_u / T = 1/(1+\tau)$ and $P_u / P = 1/(1 + \bar{\alpha}\varpi)$. Also, since $\alpha_I = \alpha_O - 1/\tau$, the inboard and outboard loading ratios are $\alpha_I = 1 - A_O / (A\tau)$ and $\alpha_O = 1 + A_I / (A\tau)$.

The solution for equal thrust of the two rotors follows from $\tau = 1$; the solution for equal power of the two rotors follows from $\bar{\alpha}\varpi = 1$. For equal thrust

$$s = \frac{1}{2\bar{\alpha}}\left(\sqrt{1 + 16\bar{\alpha}} - 1\right)$$

$$P = 2^{-3/2} (1 + \bar{\alpha} s) T v_h$$

and for equal power

$$2/(\bar{\alpha}\tau) = (1+\tau)^2$$

$$P = (1+\tau)^{-3/2} 2 T v_h$$

Table 2 gives the results for $\bar{\alpha} = 1.00$, 1.05, and 1.10 for both equal-thrust and equal-power cases. Although the difference between upper- and lower-rotor power or thrust is substantial, the momentum-theory solution is a weak function of the thrust ratio $T_u/T$, so the total power depends primarily on the nonuniform loading parameter $\bar{\alpha}$. The power is given relative to both no separation and independent rotors; the coaxial-rotor solution is closer to the no-separation case. Although it is the equal-loading case $\bar{\alpha} = 1.00$ that is often found in the literature (e.g., section 3-5 of ref. 5), the loading on the lower rotor is far from uniform. The infinite-separation solution is an upper bound on the hover performance of the coaxial

configuration. The hovering coaxial rotor has at most 7–8% less induced power than the case of no vertical separation.

A simple alternate approach is to consider the area of the lower rotor that is outside the upper-rotor slipstream as an extra active area of the rotor system (ref. 6). Thus for large separation the effective area is $\frac{3}{2}A$, and $P = T\sqrt{T/(2\rho(3/2)A)} = (2/3)^{1/2}Tv_h = 0.8165Tv_h$. For finite spacing with contraction ratio $x$, the effective area is $A_e = (2-x^2)A$, and $P = T\sqrt{T/(2\rho A_e)} = (2-x^2)^{-1/2}Tv_h = 0.8847Tv_h$ for 85% contraction. Reference 6 finds this result consistent with measurements that show the figure of merit for coaxial rotors to be 8–11% higher than for single rotors.

**Biplane Theory for Twin Rotors in Cruise**

In forward flight, the biplane effect reduces the induced power of twin rotors at moderate speed, compared to the induced power for no separation. From Munk's stagger theorem, this reduction occurs for tandem as well as coaxial configurations, as long as the vertical separation is measured in the wake.

The induced drag of a system of wings can be calculated from the energy in the far wake. For the ideal case, there is no rollup or distortion of the wake vorticity, so the wake far downstream is represented by potential jumps on lines that are projections of the wing geometry. The induced drag is

$$D_i = -\frac{\rho U^2}{2}\int \phi \frac{\partial \phi}{\partial n} dS$$

where $U$ is the free-stream velocity, $\phi$ the velocity potential, and $S$ the cross-section area of the wake with normal $n$ (ref. 7). The increment in potential across the wake surface is related to the wing-bound circulation $\Gamma$: $\Delta\phi_{wake} = \int \gamma\, dx = \Gamma/U$ (integrating over the chord); and the normal derivative $\partial\phi/\partial n$ is the induced velocity $v$ at the wake:

$$\frac{\partial \phi}{\partial n} = \pm\phi_z = \pm v = \mp\frac{1}{2\pi U}\int \frac{d\Gamma}{d\eta}\frac{d\eta}{y-\eta}$$

Thus

$$D_i = \frac{\rho}{2}\int \Gamma v\, dy = \frac{1}{2U}\int \ell v\, dy$$

where $\ell$ is the wing-section lift at span position $y$. This result is not derived with any assumption about the geometry of the wake surfaces far downstream. Hence for multiple wings, the induced drag is the sum of the drag on the $m$-th wing due to the wake of the $n$-th wing:

$$D_i = \sum D_{mn} = \frac{1}{2U}\sum \int \ell_m v_{mn}\, dy$$

The span loading can be written as a series:

$$\ell = \rho U^2 b \sum A_k \sin(k\theta) = \frac{L}{\pi b/4}\sum (A_k/A_1)\sin(k\theta)$$

where $b$ is the wing span, $y = (b/2)\sin\theta$, and the wing total lift is $L = (\pi/4)\rho U^2 b^2 A_1$ (ref. 8). For the induced drag of a planar wing due to its own wake, the integration can be performed analytically:

$$D_i = \frac{L^2}{(\pi/2)\rho U^2 b^2}\sum k(A_k/A_1)^2$$

For a single planar wing, the minimum induced drag is $D_i = L^2/((\pi/2)\rho U^2 b^2)$, obtained with elliptical loading (just $A_1$). The induced power is $P_i = UD_i$.

With the idealization of a rotor as an actuator disk (circular wing), these results can be applied to a system of rotors. Switching to rotor notation, the wing lift becomes the rotor thrust $T$, speed is $V$, and the span $b$ equals the rotor diameter $2R$. The minimum induced power for a single rotor, obtained with uniform disk loading (hence elliptical span loading), is Glauert's result $P_{ideal} = T^2/2\rho AV$. In addition to neglecting the rollup and distortion of the wake (as for fixed wings), for a rotor the discretization of the wake with a finite number of blades is also neglected when the induced power is evaluated using this far-wake model. Figure 3 shows the span loading and corresponding induced power (calculated using these equations) for an articulated helicopter rotor up to an advance ratio of $V/V_{tip} = 0.4$. The span loading is far from elliptical at high advance ratio.

For twin main rotors, only the case of equal radius of the two rotors is considered here. The reference power is the ideal power of a single rotor (area $A$) with the total thrust $T$ of both rotors: $P_{ref} = T^2/2\rho AV$. The total induced power (sum of both rotors) is written $P_i = CP_{ref}$. For no separation of the rotors, vertical or lateral, $C = 1$; for large separation, $C = 1/2$. From symmetry, the lowest power is always obtained with equal thrust on the two rotors.

For the coaxial or tandem configuration, let $z/D$ be the vertical spacing of the two rotors. The wake spacing far downstream is assumed to equal $z/D$, although the aircraft pitch angle will affect the wake spacing with tandem rotors. Figure 4 shows power $P_i/P_{ref}$ as a function of vertical separation, calculated using the equations of this section. The optimum span loading was found numerically by varying the span loading in terms of the series in $\theta$ (from symmetry, the loading is the same on the two wings). For comparison, the induced power obtained assuming elliptical loading on each wing is shown (this is the optimum solution for zero and infinite

spacing). Also shown in figure 4 is Prandtl's biplane result for elliptical loading (quoted in ref. 8, in terms of the interference factor $\sigma = 2C-1$). Based on the idea that the wing influences a volume of air contained in a cylinder circumscribing the wing tips, Stepniewski (ref. 9) proposed that the tandem rotor interference be estimated from the overlap area $mA$ of the cylinders about the two wings. Taking the effective area as $A_e = A(2-m)$ gives $C = 1/(2-m)$. While a simple result, this approach does not give as large an effect as does biplane theory; for example, it gives $P_i/P_{ref} = 0.8677$ at $z/D = 0.12$. Figure 5 compares the optimum loading and elliptical loading for $z/D = 0.12$. Table 3 shows the calculated values of $P_i/P_{ref}$ for the vertical spacings considered in this paper ($z/D = 0.06$ and 0.12), as well as for the XH-59A and Ka-26 coaxial helicopters. The benefit of the vertical spacing is 8–20% reduction in induced power (compared to zero spacing), which is a significant effect at low speed, but is overwhelmed by the effect of nonelliptical span loading at high speed.

For the side-by-side configuration, let $d/D$ be the lateral separation of the two rotors; the vertical separation is zero. Figure 6 shows power $P_i/P_{ref}$ as a function of lateral separation. The optimum span loading was found numerically for $d/D > 1$. (from symmetry, the loading is the same on the two wings). For $d/D < 1$, the optimum loading is elliptical for the two rotors combined, hence $C = 1/(1+d/D)^2$; this loading is not, however, a practical loading for $d/D$ near 1.0. For comparison, the induced power obtained assuming elliptical loading on each wing is shown (this solution is the optimum solution for zero and infinite spacing). The increased effective span of the side-by-side configuration significantly reduces the induced power.

### Performance Metrics

The following performance metrics are used in this paper. In these definitions, $W$ is the aircraft weight; $V$ the cruise speed; $T$ the total thrust of both rotors; $P$ the total aircraft power (rotor-shaft power in hover, rotor and propeller power in cruise); and $A$ is the area of one rotor.

a) Hover figure of merit: $FM = \left(T\sqrt{T/2\rho A_p}\right)/P$, where $A_p = (2-m)A$ is the projected disk area ($m$ is the overlap ratio; $m = 1$ for coaxial and $m = 0$ for no overlap). Thus for coaxial rotors the reference power is the ideal induced power of a single rotor of area A (the limit of no vertical separation).

b) Rotor effective lift-to-drag ratio: $L/D_e = LV/(P_i+P_o)$. Here $L$ is the wind-axis total rotor lift. The effective lift-to-drag ratio is a measure of rotor efficiency since the rotor parasite power is excluded.

c) Rotor-induced power: $P/P_{ref}$, reference power $P_{ref} = T\sqrt{T/2\rho A_p}$ in hover (as for figure of merit) and $P_{ref} = T^2/(2\rho AV)$ in cruise. The cruise reference is thus the ideal induced power of a single rotor of area $A$, carrying the total rotor thrust $T$ (the limit of no separation, vertical or longitudinal or lateral). Generally it is best to use as the reference power the ideal momentum-theory power of the actual rotor configuration, i.e., including the effect of vertical or lateral separation of the two rotors. However, using a reference power independent of rotor separation for the present investigation means $P/P_{ref}$ provides an absolute comparison of induced powers.

d) Rotor profile power: mean $c_d = 8(C_{Po}/\sigma)/f(\mu)$, where $f(\mu) \cong 1+4.5\mu^2+1.61\mu^{3.7}$ (ref. 5) accounts for the increase in mean dynamic pressure with advance ratio. For the cruise design condition, $\mu = 0.70$ gives $f = 3.64$.

e) Aircraft lift-to-drag ratio: $L/D = WV/P$. Here only the rotor-shaft power and auxiliary-propulsion power are included in the total power $P$; other losses are not considered.

## PERFORMANCE CALCULATION

### Analysis

Rotor performance was calculated using the comprehensive rotorcraft analysis CAMRAD II (ref. 10). CAMRAD II is an aeromechanics analysis of rotorcraft that incorporates a combination of advanced technologies, including multibody dynamics, nonlinear finite elements, and rotorcraft aerodynamics. The rotor structural-dynamics model is based on beam theory, with exact kinematics for rigid-body and joint motions. The rotor-aerodynamics model is based on second-order lifting-line theory (steady two-dimensional airfoil characteristics plus vortex wake), with unsteady aerodynamic forces from thin airfoil theory, and corrections for yawed-flow and swept blades. The aerodynamic model includes a wake analysis to calculate the rotor nonuniform-induced velocities, using rigid, prescribed, or free-wake geometry. The rotor wake is represented by a vortex lattice, with a small viscous core for tip vortices and modeling of the wake-rollup process.

The trim task finds the equilibrium solution for a steady-state operating condition, and produces the solution for performance, loads, and vibration. CAMRAD II has undergone extensive correlation of performance measurements on helicopters (ref. 10). Correlation for coaxial and tandem rotors is presented in the following section.

Rotor performance was calculated using nonuniform inflow with prescribed wake geometry in high-speed cruise and free-wake geometry in hover. Rotor/wing interference was accounted for using a vortex-wake model for both the rotor and the wing. The hover free wake included complete interaction between the wakes of the two rotors. The blade was modeled using 17 aerodynamic panels, with width ranging from 8%R at the root to 3%R at the tip. Using a combination of Reynolds number correction and drag increments for the airfoil-table data, the rotor mean drag coefficient of the baseline design is $c_d = 0.0090$ at the hover design condition. The forward-flight wake model used a tip-vortex core radius of 50% chord. The hover wake model used a tip-vortex core radius of 20% chord initially, growing quadradically with wake age to 120% chord after one revolution. An elastic-blade model was used, based on the lift-offset rotor design of reference 2, with fundamental flap and lag frequencies of 1.55/rev and 1.50/rev, respectively at hover rotor speed.

In cruise, the rotors are trimmed such that the net vertical force of both rotors and the wing equals the aircraft weight; the rotor-lift offset equals the specified value; the rotor mean roll moment and both mean and differential pitch moments are zero; and the wing lift equals the specified lift share. The lift offset is defined as $\Delta M_x/LR$, where $\Delta M_x$ is the differential rotor roll moment, and $L$ is the sum of the lift of both rotors. It was established for the work in reference 2 that trimming to zero hub moments (except for differential roll moment) gives the best performance. The variables adjusted to achieve this trim are rotor mean collective, lateral and longitudinal cyclic of each rotor, and the wing pitch angle. The trim calculation is performed for fixed pitch angle of the rotor shaft, as determined for best performance, while the wing pitch angle is trimmed to obtain the required wing lift. The calculation for this trim state gives the rotor-shaft power, rotor drag force, and wing drag force. Adding the fuselage and hub drag gives the required propeller propulsive force, from which the propeller shaft power is determined, hence the total aircraft power (exclusive of losses).

In hover, mean and differential rotor collective are adjusted such that the net rotor thrust equals the aircraft weight, and the net torque of the two rotors is equal.

**Coaxial Correlation**

Table 4 summarizes the coaxial rotors used for correlation of measured and calculated performance. Harrington (ref. 11) tested two coaxial rotors in hover, and Dingeldein (ref. 12) tested the first rotor of Harrington in the wind tunnel. The two rotors differ significantly in solidity and planform. Figures 7 and 8 compare calculated and measured hover performance for rotor#1 and rotor#2, respectively. Figure 9 shows the forward-flight performance. Both coaxial and single rotors were tested. Generally the calculation of performance is good, although better information about the airfoil characteristics would be useful.

The XH-59A Advancing Blade Concept demonstrator aircraft was tested in hover (ref. 13), in forward flight as a helicopter (ref. 14), and in forward flight with auxiliary propulsion (ref. 14). Figure 10 compares the calculated hover performance with flight-test results. The calculation of performance is good, although there is significant scatter in the test data. The figure of merit is higher than that of comparable single rotors, illustrating the beneficial effect of the coaxial configuration on hover performance. Figure 11 shows the forward-flight performance of the XH-59A, operated with the rotors providing all propulsive force as well as lift. The control phase (CP in figure 11) refers to the mixing of lateral and longitudinal cyclic to control the rotor. The flight tests were conducted at referred gross weights of 11,000 and 13,000 lb. The calculation of power and aircraft $L/D = WV/P$ is good. Figure 12 shows the performance of the XH-59A with auxiliary propulsion. The flight tests were conducted at gross weights from 11,900 to 13,300 lb; the calculations for 11,900 lb (shown in fig. 12) and 13,300 lb are similar. With lift offsets of 0.2 or 0.3, the calculation of the rotor effective $L/D_e$ is good. The ratio of the calculated induced power to optimum momentum theory power, $P_i/P_{opt}$, shows the improvement in efficiency produced by lift offset. Here $P_{opt} = 0.8594P_{ref}$ has been used (see table 3), so the induced power does exhibit at low speed the expected reduction associated with the coaxial configuration. Finally, profile power is shown in figure 12, in terms of the mean drag coefficient $c_d = 8(C_{Po}/\sigma)/f(\mu)$. At $\mu = 0.6$ the increase in mean dynamic pressure gives $f(\mu) = 2.86$. There is a very substantial increase in profile power with speed, even with lift offset. The mean drag coefficient increases by a factor of 2.2 at $\mu = 0.6$, hence the profile power increases

by a factor of 6.4. As a result of this profile power increase, the rotor effective $L/D_e$ decreases above 160 knots, so correlation with the XH-59A flight-test data neither demonstrates the potential of the lift-offset rotor to achieve good high-speed performance nor confirms the calculation of the rotor-induced power.

**Tandem Correlation**

Table 4 also describes the tandem rotor used for correlation of measured and calculated performance. Flight-test data for the CH-47D helicopter are given in reference 15. Figure 13 compares the calculated hover performance with flight-test results, and also with single rotor data (ref. 16). Figure 14 compares the calculated performance with forward-flight test results at three values of the tip speed and several $C_T$ levels ($C_T$ based on total disk area $2A$, not the projected area). The calculation of performance is generally good, given the difficulties obtaining rotor performance from flight-test measurements of aircraft performance.

## ROTOR PERFORMANCE OPTIMIZATION

For the baseline coaxial configuration, rotor planform (sweep and taper) and twist variations are explored to optimize the aircraft performance, balancing the efficiency at the hover and cruise conditions. The twist and taper distributions have four segments with linear variation in each, and the breaks at 0.25R, 0.50R, and 0.75R. The twist is expressed in terms of equivalent root-to-tip linear rate. The taper is expressed in terms of effective tip/root chord ratio. The sweep is defined in two segments, from 0.75R to 0.9R and from 0.9R to the tip. Twist exploration covered the range +3 to –24 deg. Taper exploration covered the range 2.0 to 0.25. Sweep exploration covered the range 0 to 35 deg.

The design choices for planform and twist, illustrated in figure 15, are as follows:

a) Twist: –3/–6/–15/–18 deg
b) Taper: 1.333/1.333/1.333/0.333
c) Sweep: 10/25 deg

where the values given run from inboard to outboard. The cruise operating condition is a shaft angle of 3 deg (tilted aft), and a lift offset of 0.25.

Figure 16 shows the hover and cruise performance for variations of the twist about the design choice. The performance is primarily sensitive to outboard twist, unless large values are used for inboard twist (not shown). In figure 16, the twist of the last segment ("tw4", 0.75R to 1.00R) has values from –12 to –24 deg; the lines are for the twist of the third segment ("tw3", 0.50R to 0.75R) being equal to that of the last segment, –3 deg more or –6 deg more. A similar variation is shown for the inboard twist. The design choice shown is a compromise between cruise and hover.

Figure 17 shows the hover and cruise performance for variations of the taper about the design choice. The performance is sensitive primarily to the outboard taper. In figure 17, the taper of the last segment ("taper4") has values of 0.667, 0.5, and 0.333 for values of the taper in the third segment from 1.5 to 0.667. A similar variation is shown for the inboard taper, with values in the second segment of 2.0, 1.5, 1.333, 1.0, and 0.75.Taper of the last segment is favorable for hover performance, while inverse taper inboard has a small but favorable effect on cruise performance.

Figure 18 shows the hover and cruise performance for variations of the sweep about the design choice. The sweep of the outboard segment (0.9R to tip) varies from 0 to 35 deg for each value of the inboard sweep ("sweep1", 0.75R to 0.9R). Sweep of the tip is favorable for hover performance, with figure of merit continuing to increase up to 35-deg sweep. The design choice is a smaller value (25 deg), based on considerations of structural loads and inter-rotor clearance. In addition, it is known that with kinks in the sweep distribution, lifting-line theory somewhat underpredicts the induced power.

Figure 19 shows the variation of cruise performance with shaft pitch angle (positive for aft tilt) at the design condition of 250 knots. The aircraft performance improves as the pitch angle increases. At 3-deg shaft tilt, the rotor-shaft power is small but positive. Figure 20 shows the variation of cruise performance with lift offset. At the design speed, most of the benefits are obtained at a lift offset of 0.25.

## COAXIAL CONFIGURATION

Figure 21 shows the cruise performance as a function of flight speed and lift offset for the coaxial configuration with the rotor planform and twist of figure 15. Table 5 provides details of the performance at the design cruise speed of 250 knots and at hover. The rotor lift share is specified as 0.8 at 250 knots, and the wing lift coefficient is kept constant as speed varies in these calculations. Above 200 knots, lift offset has a significant effect on the rotor performance, reducing the induced power and minimizing the profile power. Note the low value of

$P_i/P_{ref}$ at 100 knots, reflecting the reduction of induced power due to vertical separation of the rotors. The mean $c_d$ accounts for the basic rise of profile power with advance ratio, so it is clear that lift offset is able to delay the effects of stall beyond the design speed. Consequently, with a lift offset of 0.25, a rotor effective lift-to-drag ratio of $L/D_e = TV/(P_i+P_o) = 10.4$ is achieved at 250 knots, and an aircraft lift-to-drag ratio of $L/D = WV/P = 6.2$.

Figure 22 shows the span loading of the upper and lower rotors (viewed as circular wings) as a function of lift offset at 250 knots. The loading is far from elliptical, hence the ratio $P_i/P_{ref}$ is well above 1.0; lift offset reduces the induced power by producing a small shift of the loading to the advancing side. Figure 23 shows the span loading as a function of speed at lift offset of 0.25, illustrating the increase in asymmetry of the loading as speed increases.

Figure 24 shows the cruise performance as a function of flight speed and altitude. Figure 25 shows the corresponding blade loading $C_T/\sigma$. The design condition is $C_T/\sigma = 0.10$ at 5k/ISA+20°C. The break in blade loading vs. speed is where the rotor speed starts to reduce in order to maintain $M_{at} = 0.90$. The wing lift coefficient is kept constant as the speed changes (but varies with altitude), hence the blade loading increases at low speed. The rotor $L/D_e$ is relatively insensitive to altitude until stall occurs—at lower speeds as the blade loading increases. Thus the effect of altitude is to decrease the speed capability of the lift-offset rotor; or alternatively, to operate efficiently at higher altitudes, it is necessary to increase the blade area in order to maintain the same design blade loading.

## MODEL REQUIREMENTS

The influence of the rotor-wake model on cruise performance is shown in figure 26 for the coaxial configuration with lift offset of 0.25. The wake models are illustrated in figure 27. Only the far-wake model (for interactions with following blades) is shown; behind each blade where the induced velocity is calculated there is also a full vortex lattice. Note that the wing is modeled, as well as the two rotors; the induced velocities from all wakes are calculated at the collocation points on the blade (and on the wake elements for free-wake geometry), accounting for rotor-rotor and wing-rotor interference. The rolled-up wake model has a discrete tip vortex emanating from each blade tip, with strength defined by the peak bound-circulation and sheets of vorticity inboard (not shown). An alternative is the multiple-trailer model, which has a trailed vortex emanating from the edges of all aerodynamic panels. The final model introduces consolidation of these multiple trailers, combining adjacent trailers of the same sign into a single rolled-up line, located at the centroid of the original trailers. Figure 26 shows that free-wake geometry has almost no effect on the performance, as expected since the advance ratio is so high. The multiple-trailer model increases the induced power, reducing the lift-to-drag ratios. The consolidation model further reduces the efficiency. The multiple-trailer model produces a better calculation of blade airloads for some rotors (ref. 17), but test data for efficient lift-offset rotors will be needed to establish the best wake model for performance.

Figure 28 shows the influence of omitting the shed wake from the induced-velocity calculation. Without the shed wake, the induced power is significantly underpredicted. It is the shed wake directly behind the blade that is important, not the shed vorticity in the far wake.

The influence of the rotor-drag model is shown in figure 29. Without the radial drag term, the profile power is significantly underpredicted. Note that the factor $f(\mu)$ in $c_d = 8(C_{Po}/\sigma)/f(\mu)$ includes the radial drag contribution, hence without the radial drag in the computation of power it appears that the mean $c_d$ decreases with speed. The yawed flow correction impacts the airfoil stall and the effective Mach number at the swept tip, hence without the correction the profile power is overpredicted. While the radial drag and yawed flow corrections are empirical models, they have a significant effect on the calculated performance.

## TANDEM AND SIDE-BY-SIDE CONFIGURATIONS

Next tandem and side-by-side configurations are considered. The baseline is the coaxial configuration, with baseline vertical spacing $z/D = 0.06$. Tandem rotors with vertical spacing of $z/D = 0.06$ or 0.12 are examined, as a function of longitudinal separation $d/D = 0$ (coaxial) to 1.0 (no overlap). Side-by-side rotors with vertical spacing of $z/D = 0.06$ and 0 are examined as a function of lateral separation $d/D = 0$ (coaxial) to 1.25; with zero spacing, results are presented only for $d/D > 1$ (no overlap). With constant rotor radius, the disk loading reduces as the separation is increased, reaching 7.5 lb/ft$^2$ (half the coaxial value) at $d/D = 1$. With constant disk loading, the radius is reduced at $d/D = 1$ to a value of

$2^{-1/2}$ = 0.7071 times the coaxial value, and the rotor solidity is twice the coaxial value (the blade area is maintained, with half the disk area). Note that for hover the tandem and side-by-side configurations with $z/D$ = 0.06 are identical in these calculations. Also, the same total fuselage and hub drag is used for all configurations in cruise. The tandem configuration might have a lower hub drag than the coaxial configuration, but increased pylon drag for $z/D$ = 0.12. The side-by-side configuration would have increased drag from whatever structure supports the two rotors. Such differences in aircraft drag would influence the comparison of the configurations.

The hover and cruise performance of the coaxial configuration as a function of vertical spacing is shown in figures 30 and 31. The expected reduction in induced power and increase in hover figure of merit as the spacing increases is observed (fig. 30). The cruise performance shows less influence of vertical spacing (fig. 31), since the induced power is dominated by the lateral asymmetry of the loading.

Figures 32 and 33 and table 6 show the hover and cruise performance as a function of horizontal separation for constant rotor radius. The hover figure of merit (fig. 32) shows an initial decrease with separation, as the coaxial effect is lost. Because the disk loading decreases, the hover power decreases substantially as the separation is increased. The cruise performance (fig. 33) shows little effect of longitudinal separation of the rotors. Lateral separation of the rotors increases the effective span of the lifting system, so the side-by-side configuration has about a 10% improvement in performance for separations greater than $d/D$ = 0.5 (assuming fixed fuselage and hub drag).

Figures 34 and 35 and table 7 show the hover and cruise performance as a function of horizontal separation for constant disk loading. The hover figure of merit (fig. 34) decreases with separation, largely because of the decrease in blade aspect ratio. In cruise (fig. 35) the efficiency is degraded with constant disk loading, because of the reduced span of the lifting system and the increased rotor solidity. Although the trends in figure 35 are understandable, the calculated performance is erratic because of difficulties obtaining a converged inflow solution with very low aspect-ratio, high-solidity blades.

Figures 36 and 37 compare the cruise performance as a function of speed for four aircraft: coaxial ($z/D$ = 0.06), tandem with $d/D$ = 0.75 ($z/D$ = 0.06 and 0.12), and side-by-side with $d/D$ = 1.15 ($z/D$ = 0). Longitudinal separation has little effect on the cruise performance for constant radius, while the increased effective span of the side-by-side configuration improves the performance (assuming fixed fuselage and hub drag). Allowing the disk loading to decrease as the rotor separation increases is the best design approach.

## WING-ROTOR LIFT SHARE

At 250 knots, auxiliary propulsion is required. A small wing is used to mount the propellers, and this wing can also unload the rotor in cruise, thereby reducing the required rotor solidity. The baseline configuration has a rotor lift share of $T/W$ = 0.8 (ratio of rotor thrust to gross weight) at 250 knots, with a wing loading of 120 lb/ft$^2$. For variations in flight speed, the calculations use a constant wing lift coefficient to define the wing lift.

Figure 38 and table 8 show the influence of rotor lift share on the cruise performance of the coaxial configuration. For rotor lift share above 0.8, the wing size is kept constant (it is still needed to support the auxiliary propulsion), so the unloaded wing contributes a small drag. As the rotor lift share increases, it is necessary to increase the blade solidity in order to maintain the design cruise blade loading at $C_T/\sigma$ = 0.10. Unloading the rotor too much is not consistent with using lift offset, so rotor lift shares are considered only down to $T/W$ = 0.6. As the rotor lift share decreases, the rotor efficiency $L/D_e$ at 250 knots decreases, because both $P_i/P_{ref}$ and mean $c_d$ increase. However, the total aircraft drag decreases as the lift share decreases, and hence the aircraft lift-to-drag ratio $L/D = WV/P$ increases, reflecting the efficiency of generating lift by means of a fixed wing.

Also shown in figure 38 and table 8 is the calculated performance of a compound helicopter. The parameters of this design follow from a disk loading of $W/A$ = 15 lb/ft$^2$, wing loading $W/S$ = 100 lb/ft$^2$, hover $C_T/\sigma$ = 0.148, and wing span equal to rotor diameter (based on results of refs. 2 and 18). The rotor-blade twist is 0/0/–12/–12; the blade has uniform linear taper of 0.8 and no tip sweep. Following reference 18, the rotor lift is 10,000 lb ($T/W$ = 0.067), resulting in a small positive rotor-shaft power. The compound helicopter has total aircraft power comparable to the lift-offset rotor with 0.6 lift share, both somewhat better than the lift-offset rotor at 0.8 lift share. In order to compare lift-offset rotors and compound helicopters in terms of total aircraft metrics, it will be necessary to consider component weights as well as performance, including the basic trade between the weight of a large wing and the weight of a rotor designed to carry lift offset. Note also that the present comparison

has been made at the design environment (5k/ISA+20°C) of the lift-offset rotor. At higher altitudes the efficiency of the compound helicopter is expected to be better (ref. 2).

## CONCLUSIONS AND RECOMMENDATIONS

The calculated performance capability of coaxial rotors utilizing lift offset has been examined, including modern technology and rotor performance optimized for hover and high-speed cruise. Lift offset of about $\Delta M_x/LR$ = 0.25 is effective in reducing the rotor-induced power and minimizing the rotor profile power, resulting in a rotor effective lift-to-drag ratio of $L/D_e = TV/(P_i+P_o)$ = 10.4 and an aircraft lift-to-drag ratio of $L/D = WV/P$ = 6.2 at the design cruise conditions of 250 knots and 5k/ISA+20°C. Based on the assumptions for the rotor airfoil characteristics, the propeller propulsive efficiency, and the level of fuselage and hub drag, this calculated performance is probably somewhat optimistic.

The aerodynamic modeling requirements for performance calculations have been evaluated, including rotor wake and drag models for the high-speed flight condition. The design cruise condition is at a high advance ratio, so free-wake geometry is not required. Using multiple trailers instead of a rolled-up wake model results in a lower calculated rotor efficiency, and the wake geometry consolidation model reduces the efficiency further. The radial drag increases the power required, while the yawed flow effects on drag and stall reduce the power required. Confirmation of the adequacy of these models requires wind tunnel test data.

The influence of configuration on the performance of rotorcraft with lift-offset rotors has been explored, considering vertical separation, tandem and side-by-side configurations, and wing-rotor lift share. Hover performance is dominated by the variation of disk loading with twin-rotor separation and rotor radius (disk loading based on projected total rotor area). The expected increase in hover figure of merit for the coaxial configuration is observed in the calculated performance. Cruise performance is insensitive to longitudinal separation of the rotors, so the coaxial and tandem configurations have nearly the same power required and lift-to-drag ratio $L/D = WV/P$. Lateral separation of the rotors increases the effective span of the lifting system, so the side-by-side configuration has about a 10% improvement in performance for separations greater than $d/D$ = 0.5 (assuming fixed fuselage and hub drag). While comparing configurations for constant rotor radius means that the disk loading decreases with separation of the two rotors, the efficiency is degraded with constant disk loading because of the reduced span of the lifting system and the increased rotor solidity. As the rotor lift share $T/W$ decreases, the rotor efficiency $L/D_e$ at 250 knots decreases, but the total aircraft drag decreases and the aircraft lift-to-drag ratio $L/D = WV/P$ increases, reflecting the efficiency of generating lift by means of a fixed wing. The compound helicopter has total aircraft power comparable to the lift-offset rotor. In order to compare lift-offset rotors and compound helicopters in terms of total aircraft metrics, it will be necessary to consider component weights as well as performance.

To further this exploration of lift-offset rotors, airfoils should be designed for hover and the unique cruise environment of the blades, and the performance evaluated utilizing these new airfoils. The calculated rotor performance and wing-drag results should be incorporated in a conceptual design analysis, and the effect of configuration examined in terms of the complete aircraft, including the effect of separation and lift share on the weights. Finally, wind tunnel tests of advanced lift-offset rotors are needed in order to confirm the calculated performance and continue development of the analytical models.

## REFERENCES


1. Ruddell, A.J.; and Macrino, J.A.: Advancing Blade Concept (ABC) High Speed Development. AHS 36th Annual Forum, Washington, D.C., May 13–15, 1980.

2. Johnson, W.; Yamauchi, G. K.; and Watts, M. E.: NASA Heavy Lift Rotorcraft Systems Investigation. NASA/TP–2005-213467, Dec. 2005.

3. Eadie, W. J.; Sweeney, G.; and McClaren, H. E.: X2 Technology Applied to the Armed Attack Reconnaissance and Escort Mission. AHS 62th Annual Forum, Phoenix, Ariz., May 2006.

4. Akimov, A. I.; Butov, V. P.; Bourtsev, B. N.; and Selemenev, S. V.: Flight Investigation of Coaxial Rotor Tip Vortex Structure. AHS 50th Annual Forum, Washington, D.C., May 11–13, 1994, pp. 1431–1449.

5. Johnson, W.: Helicopter Theory. Princeton, New Jersey: Princeton University Press, 1980.

6. Bourtsev, B. N.; Kvokov, V. N.; Vainstein, I. M.; and Petrosian, E. A.: Phenomenon of a Coaxial Helicopter High Figure of Merit at Hover. 23rd European Rotorcraft Forum, Dresden, Germany, Sept. 16–18, 1997, pp. 86.1–86.11.

7. Landahl, M.; and Ashley, H.: Aerodynamics of Wings and Bodies. Reading, Massachusetts: Addison-Wesley Publishing Company, Inc., 1965.

8. Glauert, H.: The Elements of Aerofoil and Airscrew Theory. Cambridge: Cambridge University Press, 1947.

9. Stepniewski, W. Z.; and Keys, C. N.: Rotary-Wing Aerodynamics. New York: Dover Publications, Inc., 1984.

10. Johnson, W.: Rotorcraft Aeromechanics Applications of a Comprehensive Analysis. Heli Japan 98: AHS International Meeting on Advanced Rotorcraft Technology and Disaster Relief, Gifu, Japan, Apr. 21–23, 1998.

11. Harrington, R. D.: Full-Scale-Tunnel Investigation of the Static-Thrust Performance of a Coaxial Helicopter Rotor. NACA TN 2318, Mar. 1951.

12. Dingeldein, R. C.: Wind-Tunnel Studies of the Performance of Multirotor Configurations. NACA TN 3236, Aug. 1954.

13. Arents, D. N.: An Assessment of the Hover Performance of the XH-59A Advancing Blade Concept Demonstration Helicopter. USAAMRDL TN-25, May 1977.

14. Ruddell, A. J.: Advancing Blade Concept (ABC) Technology Demonstrator. USAAVRADCOM TR 81-D-5, Apr. 1981.

15. Bender, G. L.; Yamakawa, G. M.; Herbst, M. K.; Sullivan, P. J.; Robbins, R. D.; and Williams, R. A.: Airworthiness and Flight Characteristics Test (A&FC) of the CH-47D Helicopter: Final Report. USAAEFA Project No. 82-07, Feb. 1984.

16. Kocurek, J. D.; Berkowitz, L. F.; and Harris, F. D.: Hover Performance Methodology at Bell Helicopter Textron. AHS 36th Annual Forum, Washington, D.C., May 13–15, 1980, 48 pp.

17. Yeo, H.; and Johnson, W.: Assessment of Comprehensive Analysis Calculation of Airloads on Helicopter Rotors. J. Aircraft, vol. 42, no. 5, Sept.–Oct. 2005, pp. 1218–1228.

18. Yeo, H.; and Johnson, W.: Optimum Design of a Compound Helicopter. Heli Japan 2006, AHS International Meeting on Advanced Rotorcraft Technology and Life Saving Activities, Nagoya, Japan, Nov. 15–17, 2006.

TABLE 1. PARAMETERS OF BASELINE COAXIAL ROTORCRAFT CONFIGURATION

| | |
|---|---|
| Gross weight (lb) | 150000 |
| Hover and cruise atmosphere | 5k ISA+20°C |
| Cruise speed (kt) | 250 |
| Rotor diameter (ft) | 112.8 |
| Disk loading $W/A$ (lb/ft$^2$) | 15 |
| Cruise $C_T/\sigma$ | 0.100 |
| Maximum $M_{at}$ | 0.90 |
| cruise tip speed (ft/sec) | 600 |
| advance ratio, $V/V_{tip}$ | 0.70 |
| Hover tip speed (ft/sec) | 700 |
| cruise/hover rotor speed | 0.86 |
| hover $C_W/\sigma$ | 0.092 |
| Solidity (one rotor) | 0.0871 |
| Number blades per rotor | 4 |
| chord (75%R, ft) | 3.86 |
| Fuselage+hub drag $D/q$ (ft$^2$) | 50.0 |
| $(D/q)/(W/1000)^{2/3}$ | 1.77 |
| Wing loading (lb/ft$^2$) | 120 |
| area (ft$^2$) | 250 |
| span (ft) | 38.7 |
| cruise wing lift coefficient | 0.7 |
| Propeller propulsive efficiency | 0.9 |
| Vertical spacing, $z/D$ | 0.06 |

TABLE 2. MOMENTUM THEORY FOR COAXIAL ROTORS IN HOVER

| | | | power reference $P_{ref}$ | |
|---|---|---|---|---|
| | | | no sep | ind. rotors |
| | $T_u/T$ | $P_u/P$ | $P_i/P_{ref}$ | $P_i/P_{ref}$ |
| no separation | 0.5 | 0.5 | 1.0 | 1.4142 |
| infinite separation | | | | |
| $\overline{\alpha} = 1.10$ | | | | |
| equal $T$ | 0.5 | 0.3765 | 0.9382 | 1.3282 |
| equal $P$ | 0.6024 | 0.5 | 0.9352 | 1.3226 |
| $\overline{\alpha} = 1.05$ | | | | |
| equal $T$ | 0.5 | 0.3832 | 0.9226 | 1.3048 |
| equal $P$ | 0.5962 | 0.5 | 0.9208 | 1.3022 |
| $\overline{\alpha} = 1.00$ | | | | |
| equal $T$ | 0.5 | 0.3904 | 0.9056 | 1.2808 |
| equal $P$ | 0.5898 | 0.5 | 0.9058 | 1.2810 |
| Ind. rotors | 0.5 | 0.5 | 0.7071 | 1.0 |

TABLE 3. IDEAL INDUCED POWER FOR COAXIAL AND TANDEM ROTORS IN FORWARD FLIGHT

| | | elliptical loading | optimum loading |
|---|---|---|---|
| | $z/D$ | $P_i/P_{ref}$ | $P_i/P_{ref}$ |
| | 0.06 | 0.8779 | 0.8724 |
| XH-59A | 0.0694 | 0.8650 | 0.8594 |
| Ka-26 | 0.09 | 0.8397 | 0.8339 |
| | 0.12 | 0.8078 | 0.8023 |

TABLE 4. COAXIAL AND TANDEM ROTORS FOR CORRELATION

| Aircraft | XH-59A | Harrington #1 | Harrington #2 | CH-47D |
|---|---|---|---|---|
| Configuration | coaxial | coaxial | coaxial | tandem |
| Radius (ft) | 18 | 12.5 | 12.5 | 30 |
| Number of blades per rotor | 3 | 2 | 2 | 3 |
| Solidity (both rotors) | 0.127 | 0.054 | 0.152 | 0.0849 |
| Twist (deg) | –10 | 0 | 0 | –12 |
| Taper ratio | 0.5 | 0.305 | 1 | 1 |
| Separation, $z/D$ | 0.0694 | 0.0932 | 0.08 | |
| Overlap, $1–d/D$ | | | | 0.35 |
| Airfoil | NACA 0026 / 63218a / 23012 | $t/c$ = 0.30 to 0.12 | $t/c$ = 0.30 to 0.15 | VR7 / VR8 |

TABLE 5. COAXIAL CONFIGURATION PERFORMANCE AS A FUNCTION OF LIFT OFFSET

| lift offset | | 0.15 | 0.20 | 0.25 | 0.30 | hover |
|---|---|---|---|---|---|---|
| flight speed | knots | 250 | 250 | 250 | 250 | 0 |
| rotor tip speed | ft/sec | 600.3 | 600.3 | 600.3 | 600.3 | 700 |
| $V/V_{tip}$ | | 0.7029 | 0.7029 | 0.7029 | 0.7029 | 0 |
| advancing tip $M_{at}$ | | 0.8997 | 0.8997 | 0.8997 | 0.8997 | 0.6163 |
| shaft pitch angle | deg | 3 | 3 | 3 | 3 | |
| collective | deg | 13.51 | 10.66 | 7.55 | 4.36 | 14.14 |
| pedal | deg | 0 | 0 | 0 | 0 | -0.33 |
| lower rotor lat cyclic | deg | 5.92 | 5.91 | 5.91 | 5.89 | |
| lower rotor long cyclic | deg | -15.95 | -12.24 | -8.09 | -3.80 | |
| upper rotor lat cyclic | deg | 6.01 | 5.91 | 5.96 | 5.92 | |
| upper rotor long cyclic | deg | -15.95 | -12.20 | -7.95 | -3.69 | |
| wing angle | deg | 6.87 | 6.86 | 6.69 | 6.56 | |
| lower rotor long flap | deg | 0.22 | 0.12 | 0.04 | -0.01 | |
| lower rotor lat flap | deg | 0.70 | 1.08 | 1.47 | 1.90 | |
| upper rotor long flap | deg | 0.19 | 0.10 | 0.02 | -0.01 | |
| upper rotor lat flap | deg | 0.70 | 1.08 | 1.48 | 1.90 | |
| lift offset, $\Delta M_x/LR$ | | 0.151 | 0.200 | 0.252 | 0.301 | |
| aircraft lift | lb | 149492 | 149972 | 149681 | 149939 | |
| total rotor lift | lb | 119585 | 120086 | 119792 | 120065 | 149874 |
| lower rotor lift | lb | 61217 | 60475 | 60101 | 59792 | 68355 |
| upper rotor lift | lb | 58368 | 59611 | 59690 | 60273 | 81519 |
| wing lift | lb | 29907 | 29886 | 29889 | 29874 | |
| aircraft drag | lb | 21311 | 20746 | 20010 | 20116 | |
| total rotor drag | lb | 10806 | 10212 | 9560 | 9728 | |
| lower rotor drag | lb | 5303 | 5132 | 4860 | 4787 | |
| upper rotor drag | lb | 5503 | 5080 | 4699 | 4940 | |
| wing drag | lb | 2000 | 2030 | 1945 | 1884 | |
| profile drag | lb | 362 | 364 | 364 | 364 | |
| induced drag | lb | 1143 | 1144 | 1137 | 1132 | |
| interference drag | lb | 494 | 522 | 444 | 387 | |
| fuselage drag | lb | 8505 | 8505 | 8505 | 8505 | |
| total rotor power | hp | 3777 | 2239 | 1470 | 969 | 21806 |
| propulsive power | hp | -8290 | -7834 | -7334 | -7463 | |
| ind+int power | hp | 4214 | 3553 | 3339 | 3312 | 19459 |
| profile power | hp | 7853 | 6520 | 5466 | 5120 | 2348 |
| $P_o+P_i$ | hp | 12067 | 10073 | 8804 | 8432 | 21806 |
| aux power ($TV/\eta$) | hp | 18166 | 17685 | 17057 | 17148 | |
| aircraft power | hp | 21943 | 19923 | 18527 | 18117 | 21806 |
| wing lift coefficient | | 0.7033 | 0.7028 | 0.7029 | 0.7025 | |
| wing drag coefficient | | 0.0470 | 0.0477 | 0.0457 | 0.0443 | |
| rotor total $C_T/\sigma$ | | 0.0997 | 0.1000 | 0.0997 | 0.0998 | 0.0919 |
| mean $c_d = 8(C_{Po}/\sigma)/f(\mu)$ | | 0.01311 | 0.01088 | 0.00913 | 0.00855 | 0.00905 |
| $P_i/P_{ref}$ | | 2.996 | 2.505 | 2.366 | 2.336 | 1.140 |
| hover figure of merit | | | | | | 0.783 |
| rotor $L/D_e = LV/(P_o+P_i)$ | | 7.603 | 9.146 | 10.438 | 10.924 | |
| aircraft $L/D = WV/P$ | | 5.244 | 5.776 | 6.211 | 6.352 | |

TABLE 6. PERFORMANCE OF COAXIAL, TANDEM AND SIDE-BY-SIDE CONFIGURATIONS, FOR FIXED ROTOR RADIUS

| configuration | | coaxial | tandem | tandem | side-by-side | coaxial | tandem | tandem | side-by-side |
|---|---|---|---|---|---|---|---|---|---|
| separation $d/D$ | | 0 | 0.75 | 0.75 | 1.15 | | | | |
| vertical $z/D$ | | 0.06 | 0.06 | 0.12 | 0 | | | | |
| overlap area factor $m$ | | 1 | 0.1443 | 0.1443 | 0 | | | | |
| radius | ft | 56.42 | 56.42 | 56.42 | 56.42 | | | | |
| disk loading | lb/ft$^2$ | 15 | 8.08 | 8.08 | 7.50 | | | | |
| solidity (one rotor) | | 0.0871 | 0.0871 | 0.0871 | 0.0871 | | | | |
| flight speed | knots | 250 | 250 | 250 | 250 | 0 | 0 | 0 | 0 |
| rotor tip speed | ft/sec | 600.3 | 600.3 | 600.3 | 600.3 | 700 | 700 | 700 | 700 |
| $V/V_{tip}$ | | 0.7029 | 0.7029 | 0.7029 | 0.7029 | 0 | 0 | 0 | 0 |
| advancing tip $M_{at}$ | | 0.8997 | 0.8997 | 0.8997 | 0.8997 | 0.6163 | 0.6163 | 0.6163 | 0.6163 |
| shaft pitch angle | deg | 3 | 3 | 3 | 3 | | | | |
| collective | deg | 7.55 | 7.85 | 7.80 | 5.49 | 14.14 | 12.40 | 12.37 | 11.89 |
| pedal | deg | 0 | 0 | 0 | 0 | -0.33 | -0.30 | -0.33 | 0 |
| lower rotor lat cyclic | deg | 5.91 | 5.38 | 5.52 | 4.85 | | | | |
| lower rotor long cyclic | deg | -8.09 | -8.34 | -8.37 | -5.45 | | | | |
| upper rotor lat cyclic | deg | 5.96 | 5.54 | 5.54 | 4.82 | | | | |
| upper rotor long cyclic | deg | -7.95 | -8.30 | -8.21 | -5.46 | | | | |
| wing angle | deg | 6.69 | 6.51 | 6.42 | 5.52 | | | | |
| lower rotor long flap | deg | 0.04 | -0.01 | -0.05 | 0.02 | | | | |
| lower rotor lat flap | deg | 1.47 | 1.51 | 1.51 | 1.47 | | | | |
| upper rotor long flap | deg | 0.02 | 0.01 | 0.01 | 0.02 | | | | |
| upper rotor lat flap | deg | 1.48 | 1.45 | 1.45 | 1.47 | | | | |
| lift offset, $\Delta M_x/LR$ | | 0.252 | 0.250 | 0.250 | 0.250 | | | | |
| aircraft lift | lb | 149681 | 149881 | 149809 | 149715 | | | | |
| total rotor lift | lb | 119792 | 119986 | 119928 | 119747 | 149905 | 150131 | 150128 | 150135 |
| lower rotor lift | lb | 60101 | 55883 | 55904 | 59791 | 68372 | 75876 | 76570 | 75055 |
| upper rotor lift | lb | 59690 | 64103 | 64024 | 59955 | 81534 | 74255 | 73558 | 75079 |
| wing lift | lb | 29889 | 29895 | 29881 | 29968 | | | | |
| aircraft drag | lb | 20010 | 19906 | 19932 | 19097 | | | | |
| total rotor drag | lb | 9560 | 9537 | 9619 | 9131 | | | | |
| lower rotor drag | lb | 4860 | 4954 | 4907 | 4487 | | | | |
| upper rotor drag | lb | 4699 | 4583 | 4712 | 4644 | | | | |
| wing drag | lb | 1945 | 1864 | 1808 | 1461 | | | | |
| profile drag | lb | 364 | 365 | 365 | 372 | | | | |
| induced drag | lb | 1137 | 1140 | 1150 | 1120 | | | | |
| interference drag | lb | 444 | 359 | 293 | -31 | | | | |
| fuselage drag | lb | 8505 | 8505 | 8505 | 8505 | | | | |
| total rotor power | hp | 1470 | 1478 | 1369 | 753 | 21812 | 16628 | 16617 | 16644 |
| propulsive power | hp | -7334 | -7317 | -7379 | -7005 | | | | |
| ind+int power | hp | 3339 | 3351 | 3262 | 2661 | 19464 | 14332 | 14329 | 14449 |
| profile power | hp | 5466 | 5443 | 5487 | 5097 | 2348 | 2296 | 2287 | 2195 |
| $P_o+P_i$ | hp | 8804 | 8794 | 8748 | 7758 | 21812 | 16628 | 16617 | 16644 |
| aux power ($TV/\eta$) | hp | 17057 | 16968 | 16991 | 16279 | | | | |
| aircraft power | hp | 18527 | 18446 | 18360 | 17032 | 21812 | 16628 | 16617 | 16644 |
| wing lift coefficient | | 0.7029 | 0.7030 | 0.7027 | 0.7047 | | | | |
| wing drag coefficient | | 0.0457 | 0.0438 | 0.0425 | 0.0344 | | | | |
| rotor total $C_T/\sigma$ | | 0.0997 | 0.0999 | 0.0999 | 0.0998 | 0.0919 | 0.0920 | 0.0920 | 0.0920 |
| mean $c_d = 8(C_{Po}/\sigma)/f(\mu)$ | | 0.00913 | 0.00909 | 0.00916 | 0.00851 | 0.00905 | 0.00885 | 0.00881 | 0.00845 |
| $P_i/P_{ref}$ | | 2.366 | 2.352 | 2.490 | 1.646 | 1.140 | 1.141 | 1.141 | 1.194 |
| hover figure of merit | | | | | | 0.783 | 0.755 | 0.756 | 0.727 |
| rotor $L/D_e = LV/(P_o+P_i)$ | | 10.438 | 10.468 | 10.517 | 11.841 | | | | |
| aircraft $L/D = WV/P$ | | 6.211 | 6.239 | 6.268 | 6.757 | | | | |

TABLE 7. PERFORMANCE OF COAXIAL, TANDEM, AND SIDE-BY-SIDE CONFIGURATIONS, FOR FIXED DISK LOADING

| configuration | | coaxial | tandem | tandem | side-by-side | coaxial | tandem | tandem | side-by-side |
|---|---|---|---|---|---|---|---|---|---|
| separation $d/D$ | | 0 | 0.75 | 0.75 | 1.15 | | | | |
| vertical $z/D$ | | 0.06 | 0.06 | 0.12 | 0 | | | | |
| overlap area factor $m$ | | 1 | 0.1443 | 0.1443 | 0 | | | | |
| radius | ft | 56.42 | 41.42 | 41.42 | 39.89 | | | | |
| disk loading | lb/ft$^2$ | 15 | 15 | 15 | 15 | | | | |
| solidity (one rotor) | | 0.0871 | 0.1617 | 0.1617 | 0.1743 | | | | |
| flight speed | knots | 250 | 250 | 250 | 250 | 0 | 0 | 0 | 0 |
| rotor tip speed | ft/sec | 600.3 | 600.3 | 600.3 | 600.3 | 700 | 700 | 700 | 700 |
| $V/V_{tip}$ | | 0.7029 | 0.7029 | 0.7029 | 0.7029 | 0 | 0 | 0 | 0 |
| advancing tip $M_{at}$ | | 0.8997 | 0.8997 | 0.8997 | 0.8997 | 0.6163 | 0.6163 | 0.6163 | 0.6163 |
| shaft pitch angle | deg | 3 | 3 | 3 | 3 | | | | |
| collective | deg | 7.55 | 10.20 | 9.30 | 7.09 | 14.14 | 15.80 | 15.81 | 15.57 |
| pedal | deg | 0 | 0 | 0 | 0 | -0.33 | -0.40 | -0.47 | 0 |
| lower rotor lat cyclic | deg | 5.91 | 5.86 | 5.68 | 5.37 | | | | |
| lower rotor long cyclic | deg | -8.09 | -10.24 | -9.94 | -6.32 | | | | |
| upper rotor lat cyclic | deg | 5.96 | 6.22 | 5.72 | 5.41 | | | | |
| upper rotor long cyclic | deg | -7.95 | -10.15 | -8.66 | -6.24 | | | | |
| wing angle | deg | 6.69 | 6.58 | 6.58 | 5.44 | | | | |
| lower rotor long flap | deg | 0.04 | 0.00 | -0.02 | -0.01 | | | | |
| lower rotor lat flap | deg | 1.47 | 0.92 | 0.94 | 0.84 | | | | |
| upper rotor long flap | deg | 0.02 | -0.03 | 0.04 | 0.03 | | | | |
| upper rotor lat flap | deg | 1.48 | 0.91 | 0.90 | 0.83 | | | | |
| lift offset, $\Delta M_x/LR$ | | 0.252 | 0.252 | 0.250 | 0.247 | | | | |
| aircraft lift | lb | 149681 | 149049 | 150348 | 150557 | | | | |
| total rotor lift | lb | 119792 | 119061 | 120488 | 120609 | 149905 | 150131 | 150117 | 150000 |
| lower rotor lift | lb | 60101 | 50974 | 52087 | 59286 | 68372 | 76141 | 76803 | 74997 |
| upper rotor lift | lb | 59690 | 68086 | 68401 | 61323 | 81534 | 73990 | 73314 | 75003 |
| wing lift | lb | 29889 | 29988 | 29861 | 29948 | | | | |
| aircraft drag | lb | 20010 | 21562 | 16400 | 16114 | | | | |
| total rotor drag | lb | 9560 | 11155 | 6004 | 6181 | | | | |
| lower rotor drag | lb | 4860 | 5639 | 4150 | 3855 | | | | |
| upper rotor drag | lb | 4699 | 5517 | 1854 | 2326 | | | | |
| wing drag | lb | 1945 | 1902 | 1891 | 1429 | | | | |
| profile drag | lb | 364 | 367 | 365 | 372 | | | | |
| induced drag | lb | 1137 | 1144 | 1168 | 1122 | | | | |
| interference drag | lb | 444 | 390 | 358 | -66 | | | | |
| fuselage drag | lb | 8505 | 8505 | 8505 | 8505 | | | | |
| total rotor power | hp | 1470 | 4314 | 8688 | 7623 | 21812 | 23793 | 23839 | 25316 |
| propulsive power | hp | -7334 | -8558 | -4606 | -4742 | | | | |
| ind+int power | hp | 3339 | 6870 | 7315 | 6718 | 19464 | 21552 | 21617 | 23298 |
| profile power | hp | 5466 | 6002 | 5980 | 5647 | 2348 | 2241 | 2222 | 2018 |
| $P_o+P_i$ | hp | 8804 | 12872 | 13295 | 12365 | 21812 | 23793 | 23839 | 25316 |
| aux power ($TV/\eta$) | hp | 17057 | 18380 | 13980 | 13736 | | | | |
| aircraft power | hp | 18527 | 22694 | 22668 | 21359 | 21812 | 23793 | 23839 | 25316 |
| wing lift coefficient | | 0.7029 | 0.7052 | 0.7022 | 0.7042 | | | | |
| wing drag coefficient | | 0.0457 | 0.0447 | 0.0445 | 0.0336 | | | | |
| rotor total $C_T/\sigma$ | | 0.0997 | 0.0990 | 0.0999 | 0.0999 | 0.0919 | 0.0920 | 0.0920 | 0.0919 |
| mean $c_d = 8(C_{Po}/\sigma)/f(\mu)$ | | 0.00913 | 0.01002 | 0.00998 | 0.00943 | 0.00905 | 0.00863 | 0.00856 | 0.00777 |
| $P_i/P_{ref}$ | | 2.366 | 2.639 | 2.981 | 2.048 | 1.140 | 1.260 | 1.264 | 1.364 |
| hover figure of merit | | | | | | 0.783 | 0.719 | 0.717 | 0.675 |
| rotor $L/D_e = LV/(P_o+P_i)$ | | 10.438 | 7.096 | 6.953 | 7.483 | | | | |
| aircraft $L/D = WV/P$ | | 6.211 | 5.071 | 5.077 | 5.388 | | | | |

TABLE 8. COAXIAL CONFIGURATION PERFORMANCE AS A FUNCTION OF ROTOR LIFT SHARE, INCLUDING COMPOUND HELICOPTER

| configuration | | Lift offset | Lift offset | Lift offset | Compound |
|---|---|---|---|---|---|
| rotor lift share | | 1.0 | 0.8 | 0.6 | 0.067 |
| radius | ft | 56.42 | 56.42 | 56.42 | 56.42 |
| solidity (one rotor) | | 0.1089 | 0.0871 | 0.0654 | 0.0541 |
| wing span | ft | 38.73 | 38.73 | 54.77 | 112.84 |
| wing chord | ft | 6.46 | 6.46 | 9.13 | 12.41 |
| hover tip speed | ft/sec | 700 | 700 | 700 | 700 |
| hover $C_T/\sigma$ | | 0.0735 | 0.0919 | 0.1226 | 0.1480 |
| flight speed | knots | 250 | 250 | 250 | 250 |
| rotor tip speed | ft/sec | 600.3 | 600.3 | 600.3 | 600.3 |
| $V/V_{tip}$ | | 0.7029 | 0.7029 | 0.7029 | 0.7029 |
| advancing tip $M_{at}$ | | 0.8997 | 0.8997 | 0.8997 | 0.8997 |
| shaft pitch angle | deg | 3 | 3 | 3 | 3 |
| collective | deg | 7.61 | 7.47 | 6.72 | -5.43 |
| lower rotor lat cyclic | deg | 6.67 | 5.92 | 5.02 | 0.53 |
| lower rotor long cyclic | deg | -7.88 | -7.97 | -7.12 | 5.25 |
| upper rotor lat cyclic | deg | 6.85 | 5.95 | 4.87 | 0.18 |
| upper rotor long cyclic | deg | -7.79 | -7.84 | -7.07 | 5.18 |
| wing angle | deg | -1.66 | 6.68 | 6.51 | 4.04 |
| lower rotor long flap | deg | -0.04 | 0.04 | 0.08 | 0.15 |
| lower rotor lat flap | deg | 1.88 | 1.48 | 1.09 | -0.35 |
| upper rotor long flap | deg | -0.05 | 0.03 | 0.05 | 0.12 |
| upper rotor lat flap | deg | 1.88 | 1.47 | 1.07 | -0.33 |
| lift offset, $\Delta M_x/LR$ | | 0.253 | 0.250 | 0.252 | 0 |
| aircraft lift | lb | 150190 | 150211 | 149714 | 149485 |
| total rotor lift | lb | 149180 | 120338 | 89899 | 9628 |
| lower rotor lift | lb | 75609 | 60415 | 45132 | 5046 |
| upper rotor lift | lb | 73572 | 59923 | 44767 | 4582 |
| wing lift | lb | 1010 | 29874 | 59815 | 139857 |
| aircraft drag | lb | 20746 | 19889 | 19602 | 17241 |
| total rotor drag | lb | 11901 | 9443 | 7459 | 3375 |
| lower rotor drag | lb | 5762 | 4741 | 3761 | 1662 |
| upper rotor drag | lb | 6139 | 4702 | 3699 | 1713 |
| wing drag | lb | 340 | 1941 | 3638 | 5360 |
| profile drag | lb | 333 | 364 | 682 | 1735 |
| induced drag | lb | 9 | 1135 | 2262 | 2951 |
| interference drag | lb | -2 | 442 | 694 | 674 |
| fuselage drag | lb | 8505 | 8505 | 8505 | 8505 |
| total rotor power | hp | 1676 | 1555 | 944 | 2943 |
| propulsive power | hp | -9130 | -7244 | -5723 | -2590 |
| ind+int power | hp | 4304 | 3373 | 2418 | 555 |
| profile power | hp | 6503 | 5426 | 4249 | 4978 |
| $P_o+P_i$ | hp | 10806 | 8799 | 6667 | 5533 |
| aux power ($TV/\eta$) | hp | 17684 | 16954 | 16709 | 14696 |
| aircraft power | hp | 19360 | 18509 | 17653 | 17639 |
| wing lift coefficient | | 0.0237 | 0.7025 | 0.7033 | 0.5873 |
| wing drag coefficient | | 0.0080 | 0.0457 | 0.0428 | 0.0225 |
| rotor total $C_T/\sigma$ | | 0.0992 | 0.1001 | 0.0999 | 0.0131 |
| mean $c_d = 8(C_{Po}/\sigma)/f(\mu)$ | | 0.00869 | 0.00906 | 0.00946 | 0.01338 |
| $P_i/P_{ref}$ | | 1.954 | 2.353 | 3.023 | 60.467 |
| rotor $L/D_e = LV/(P_o+P_i)$ | | 10.591 | 10.492 | 10.346 | 1.335 |
| aircraft $L/D = WV/P$ | | 5.944 | 6.217 | 6.519 | 6.524 |

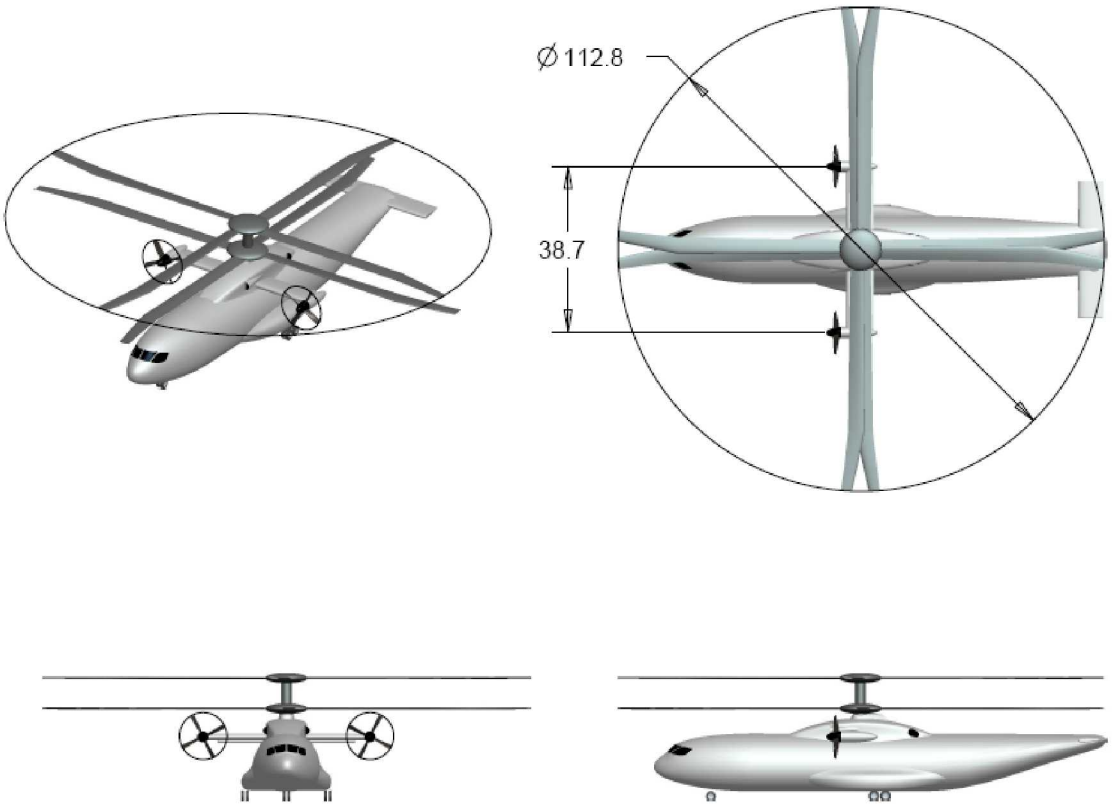


Figure 1. Illustration of baseline coaxial rotorcraft configuration, utilizing lift-offset rotors (courtesy G. Nunez, AFDD).

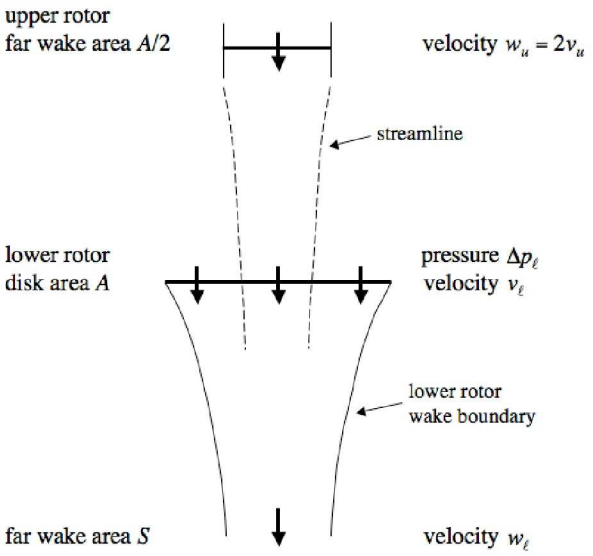


Figure 2. Momentum-theory model of coaxial rotors in hover, for lower rotor far below upper rotor, showing velocities and areas in flow field and pressure on rotor disk. Velocities $w_u$ and $w_\ell$ are uniform across wake section; pressure $\Delta p_\ell$ and velocity $v_\ell$ at lower-rotor disk are not uniform.

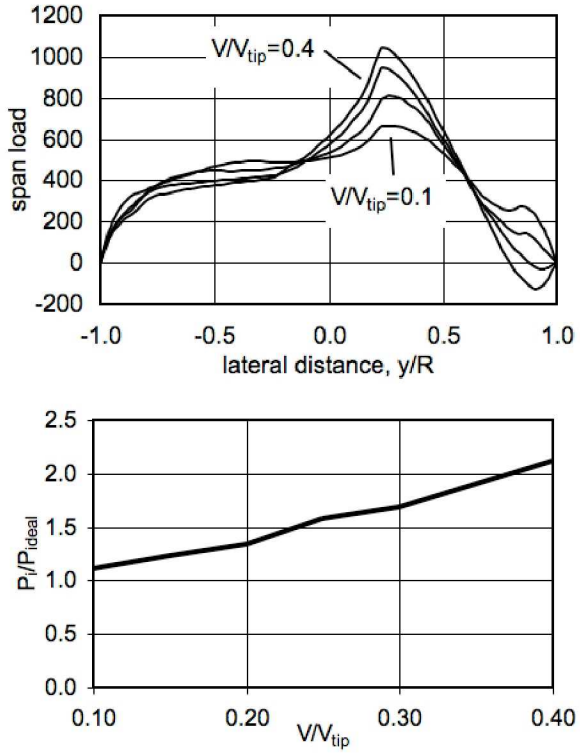


Figure 3. Span loading and corresponding induced power of articulated helicopter rotor.

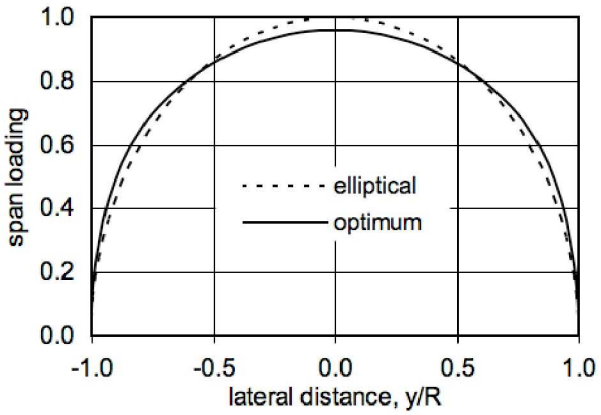


Figure 5. Span loading for ideal induced power in forward flight, twin-rotor vertical spacing $z/D = 0.12$.

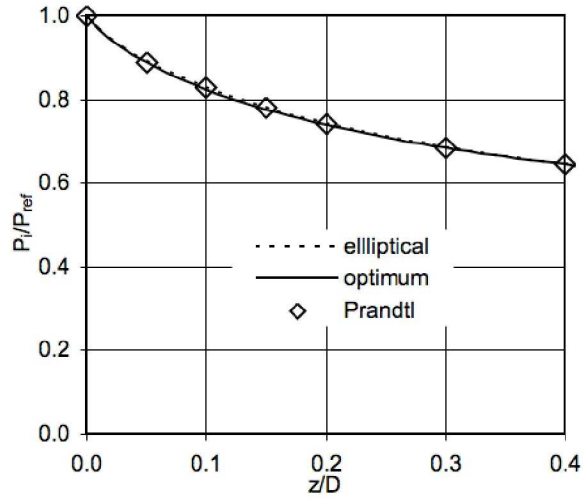


Figure 4. Ideal induced power in forward flight as a function of twin-rotor vertical spacing.

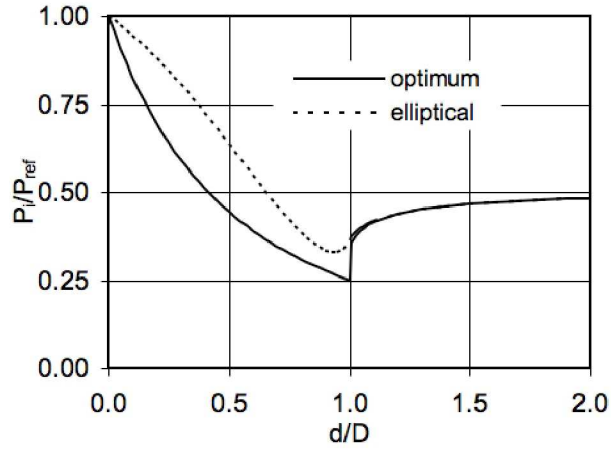


Figure 6. Ideal induced power in forward flight as a function of twin-rotor lateral spacing.

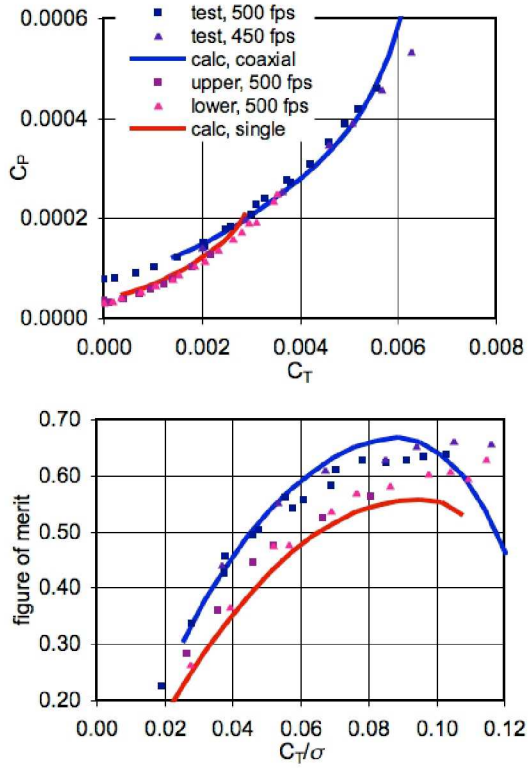


Figure 7. Hover performance of Harrington rotor#1.

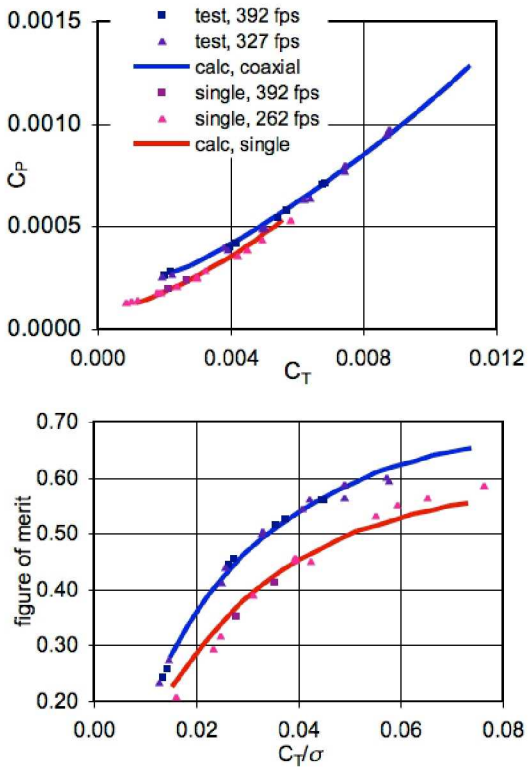


Figure 8. Hover performance of Harrington rotor#2.

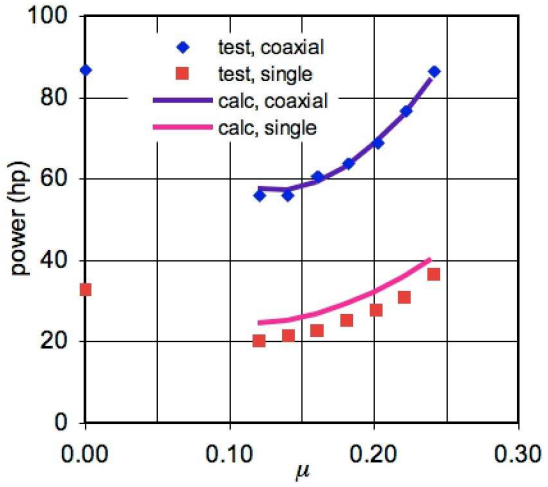


Figure 9. Forward-flight performance of Harrington rotor#1 at $C_T/\sigma = 0.089$.

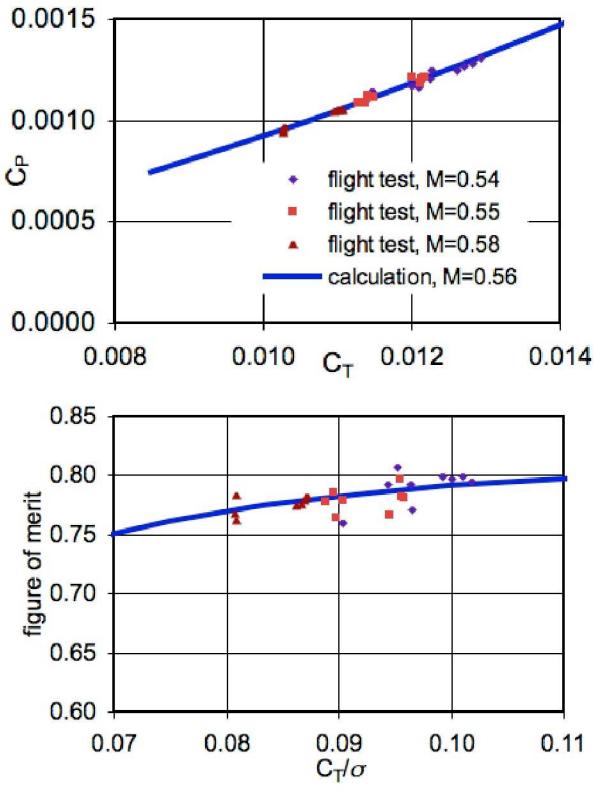


Figure 10. Hover performance of XH-59A.

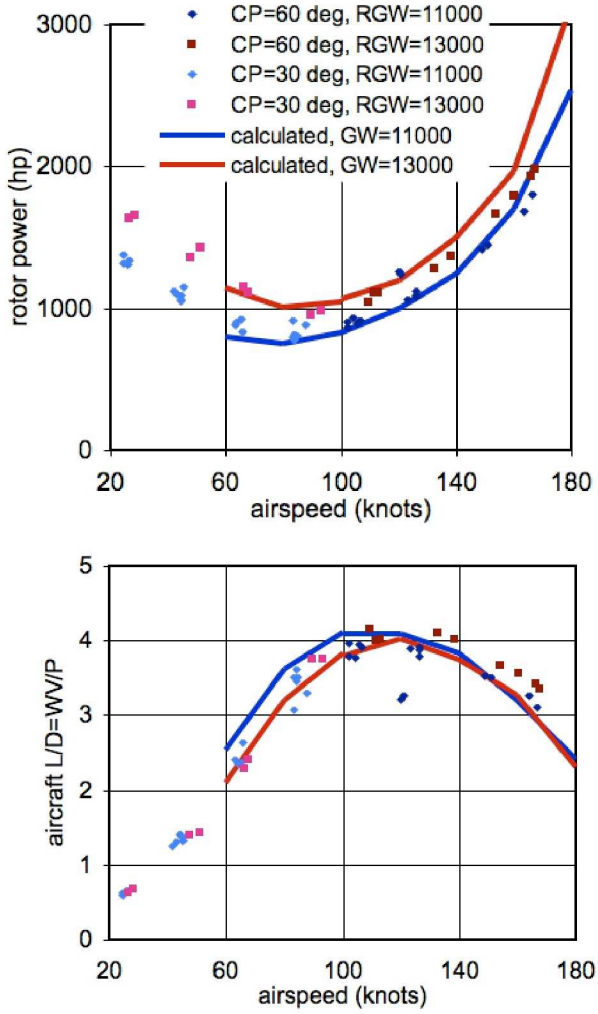


Figure 11. Forward-flight performance of XH-59A (without auxiliary propulsion).

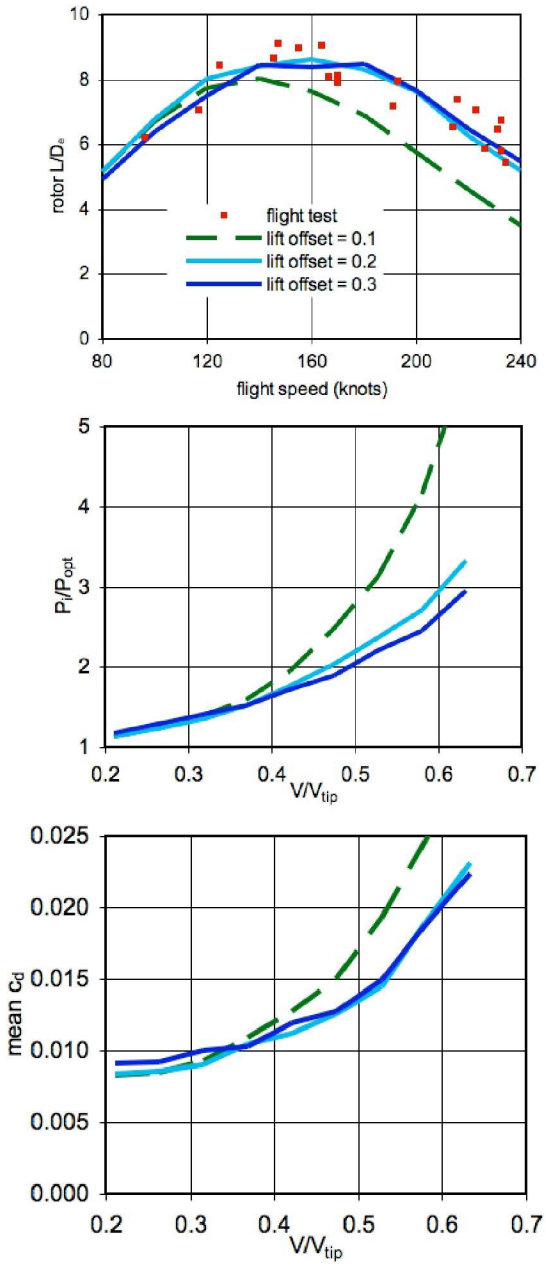


Figure 12. Forward-flight performance of XH-59A with auxiliary propulsion.

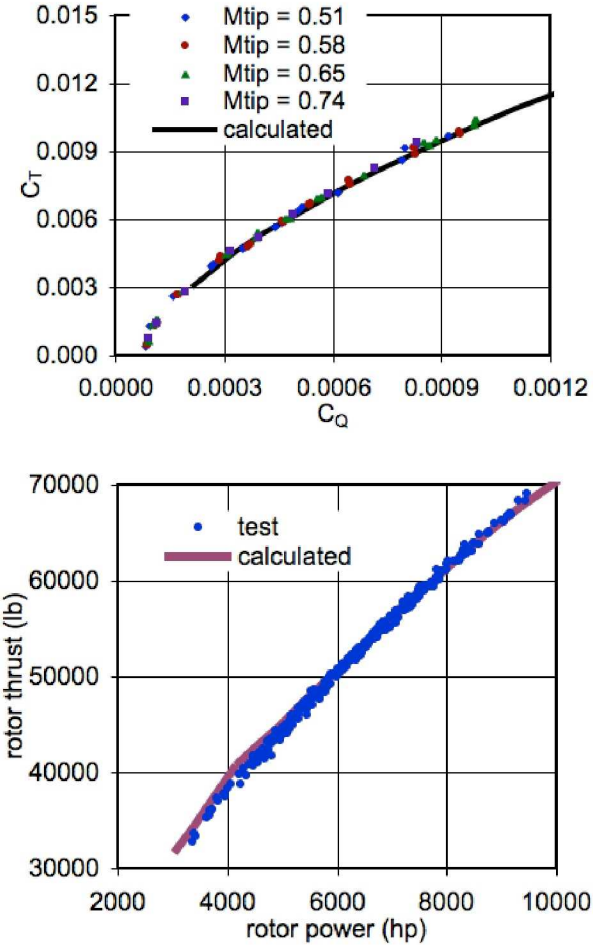


Figure 13. Hover performance of CH-47D: single rotor on whirl stand (top) and tandem rotors in flight (bottom).

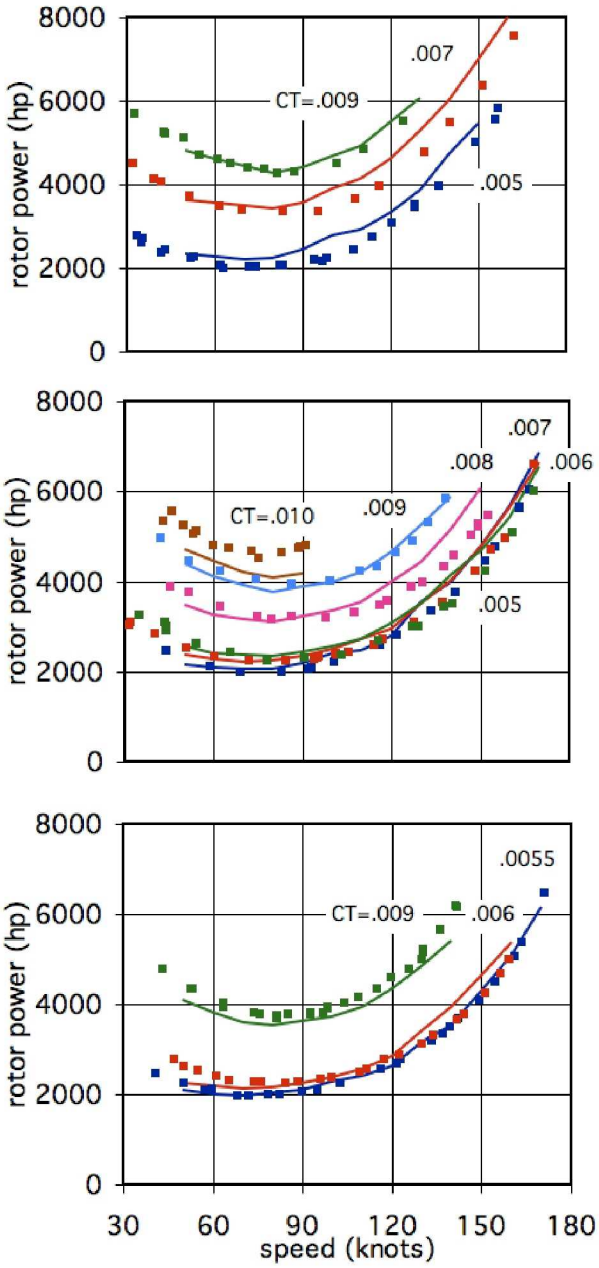


Figure 14. Forward-flight performance of CH-47D helicopter; $M_{tip}$ = 0.69 (top), 0.63, and 0.60 (bottom).

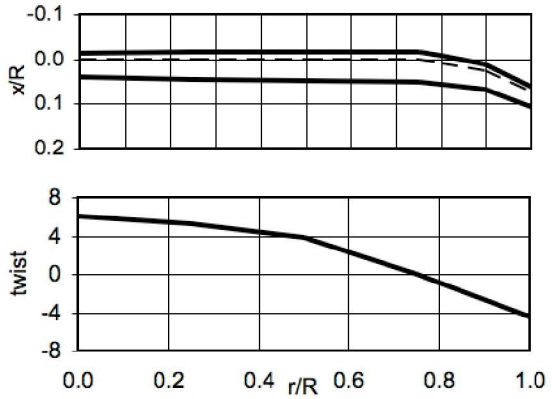


Figure 15. Rotor-blade planform and twist, designed for hover and cruise conditions of coaxial configuration.

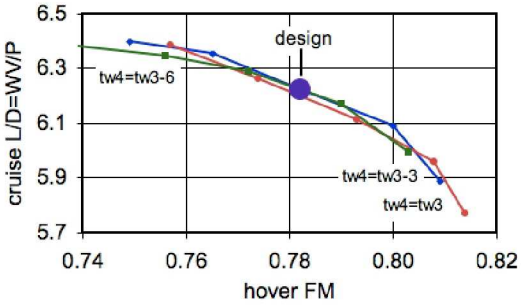


a) outboard twist

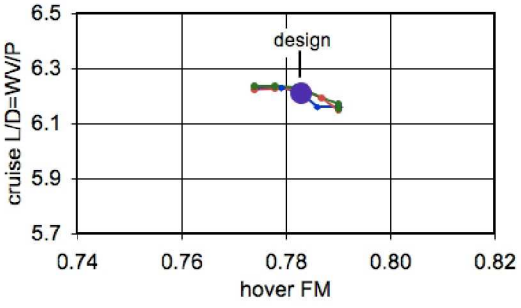


b) inboard twist

Figure 16. Influence of twist on hover and cruise performance (baseline coaxial configuration).

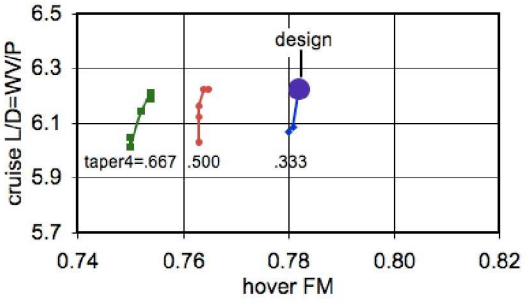


a) outboard taper

Figure 17. Influence of taper on hover and cruise performance (baseline coaxial configuration).

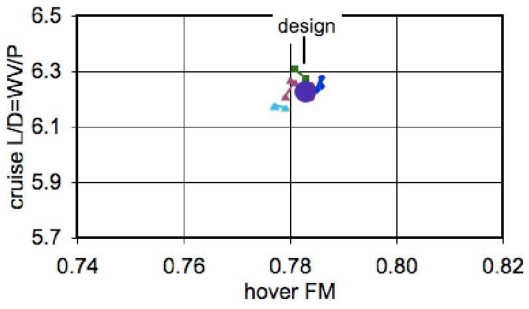


b) inboard taper

Figure 17. Concluded.

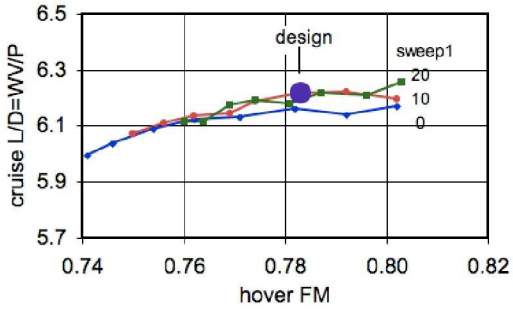


Figure 18. Influence of tip sweep on hover and cruise performance (baseline coaxial configuration).

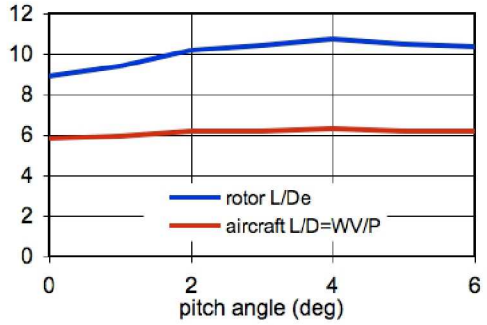


Figure 19. Influence of rotor-shaft angle on cruise performance at 250 knots.

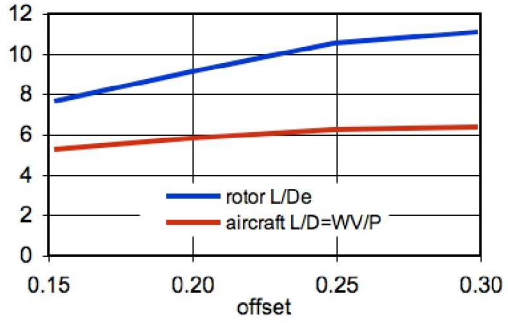


Figure 20. Influence of lift offset on cruise performance at 250 knots.

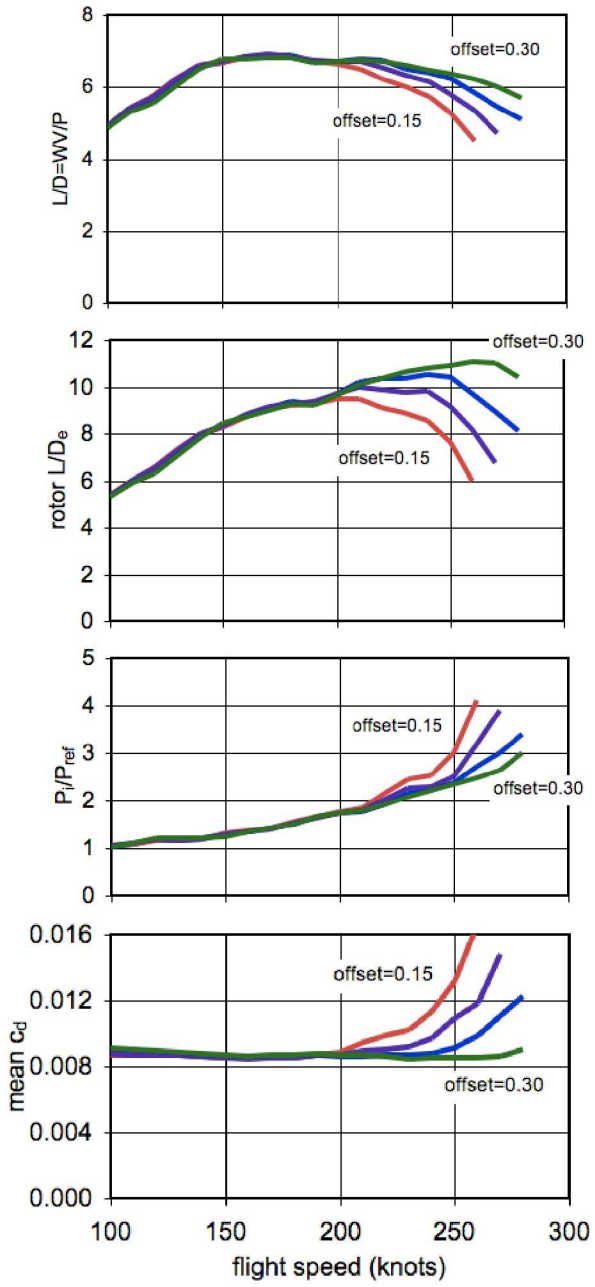


Figure 21. Cruise performance of coaxial lift-offset rotorcraft.

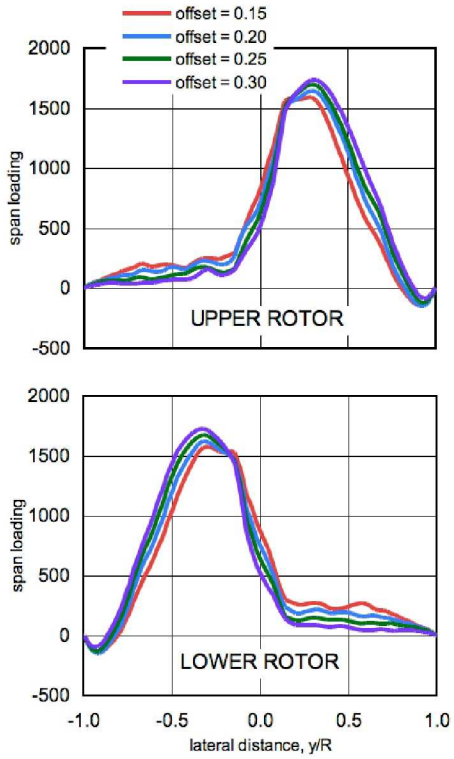


Figure 22. Span loading as a function of lift offset; $V = 250$ knots.

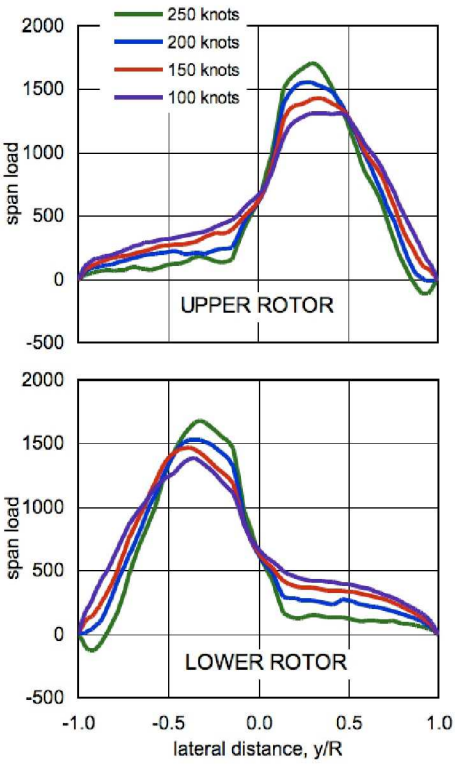


Figure 23. Span loading as a function of speed; offset = 0.25.

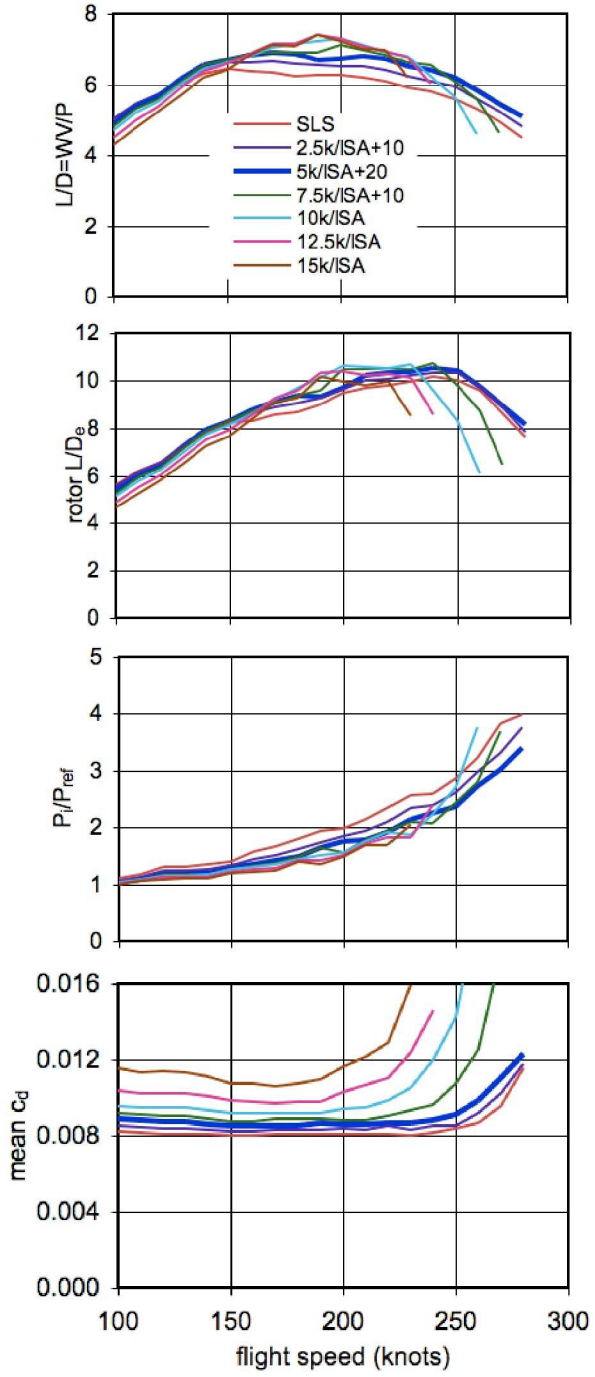


Figure 24. Cruise performance as a function of altitude.

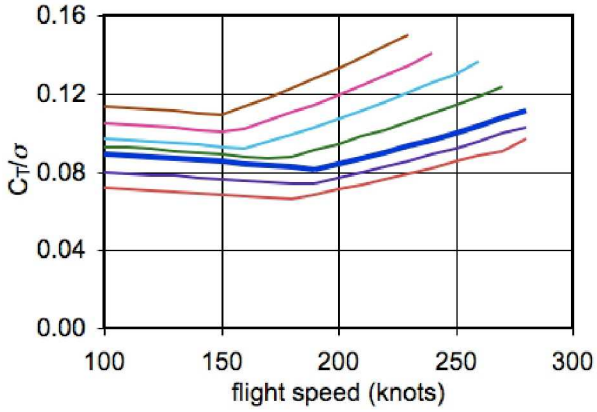


Figure 25. Rotor-blade loading $C_T/\sigma$ as a function of speed and altitude.

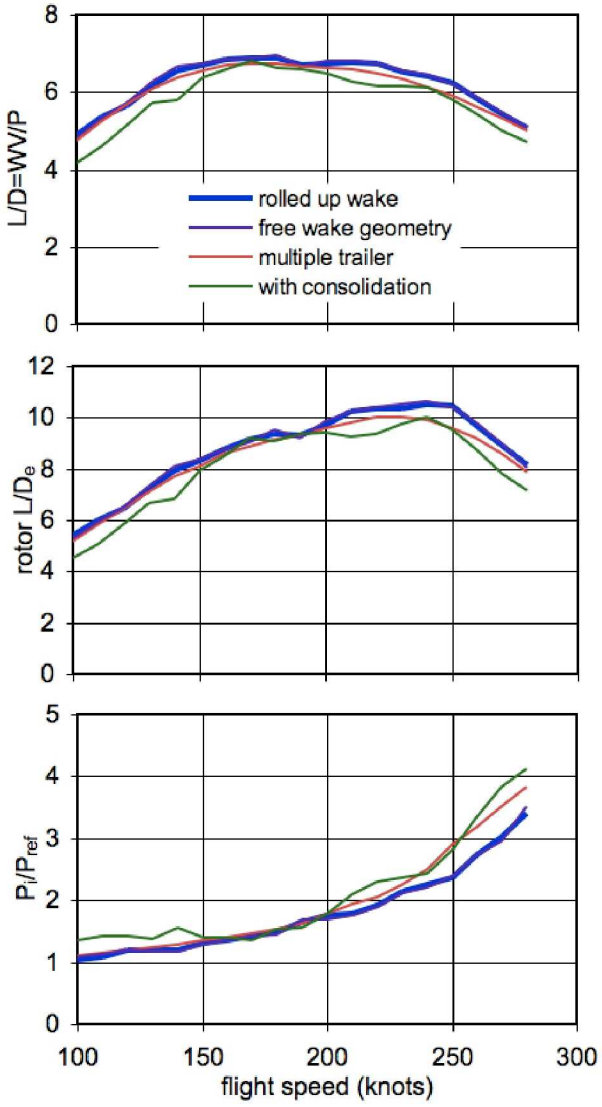


Figure 26. Influence of rotor-wake model on cruise performance.

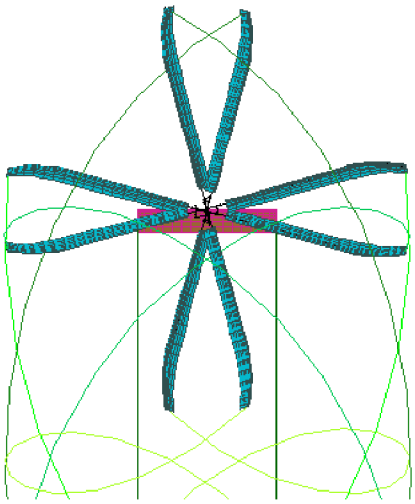

a) Rigid-wake geometry; rolled-up model.

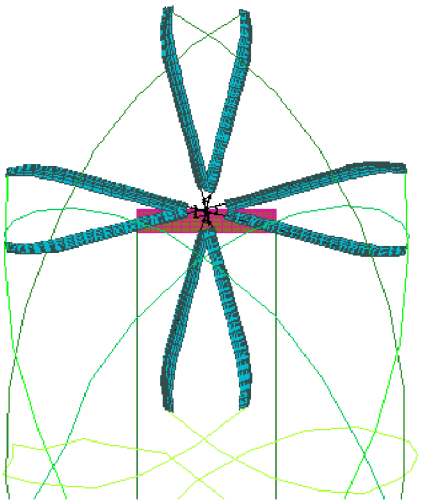

b) Free-wake geometry; rolled-up model.

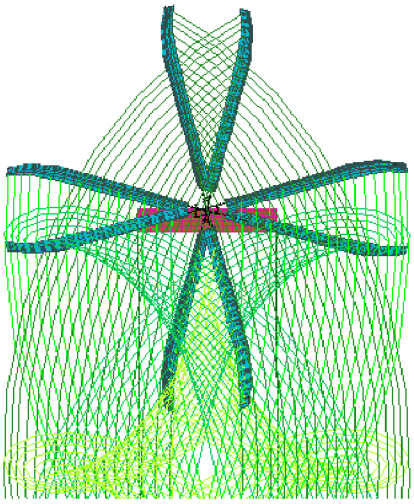

c) Rigid-wake geometry; multiple-trailer model.

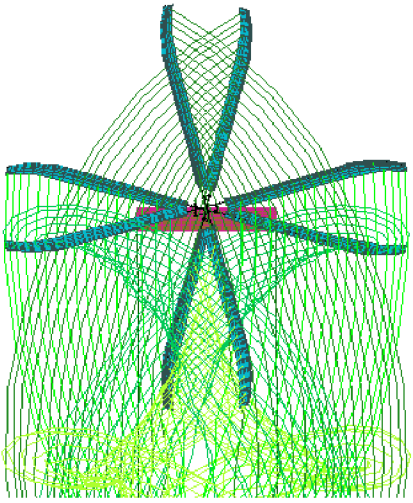

d) Free-wake geometry; multiple-trailer model.

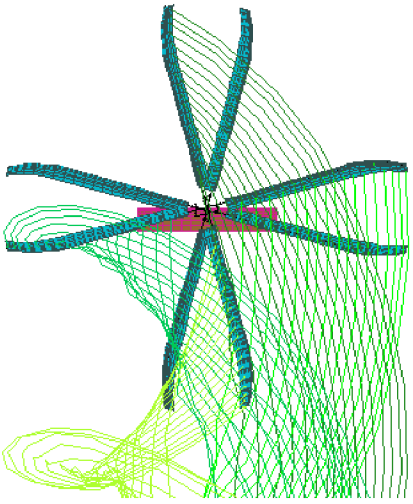

e) Free-wake geometry; multiple-trailer model (only upper rotor shown).

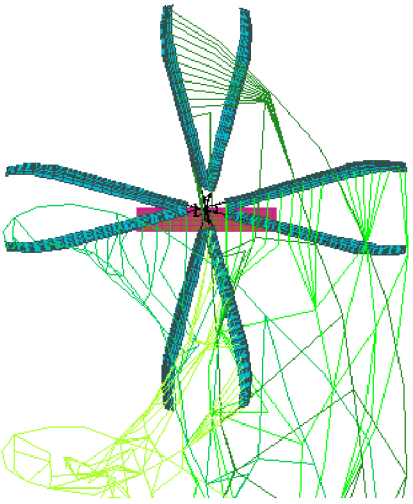

f) Free-wake geometry; multiple-trailer model with consolidation (only upper rotor shown).

Figure 27. Rotor-wake models, $V = 250$ knots, $V/V_{tip} = 0.70$; trailed vorticity of two rotors and wing.

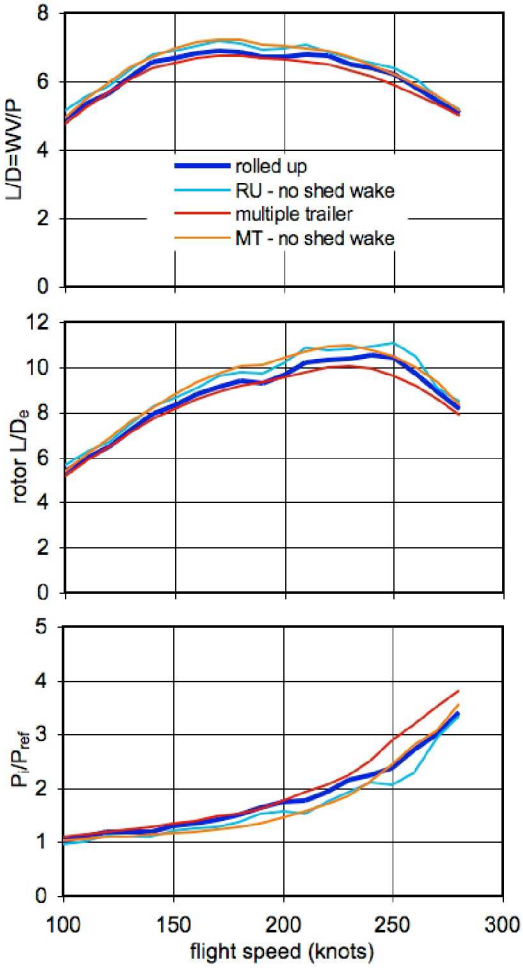


Figure 28. Influence of rotor-wake model on cruise performance.

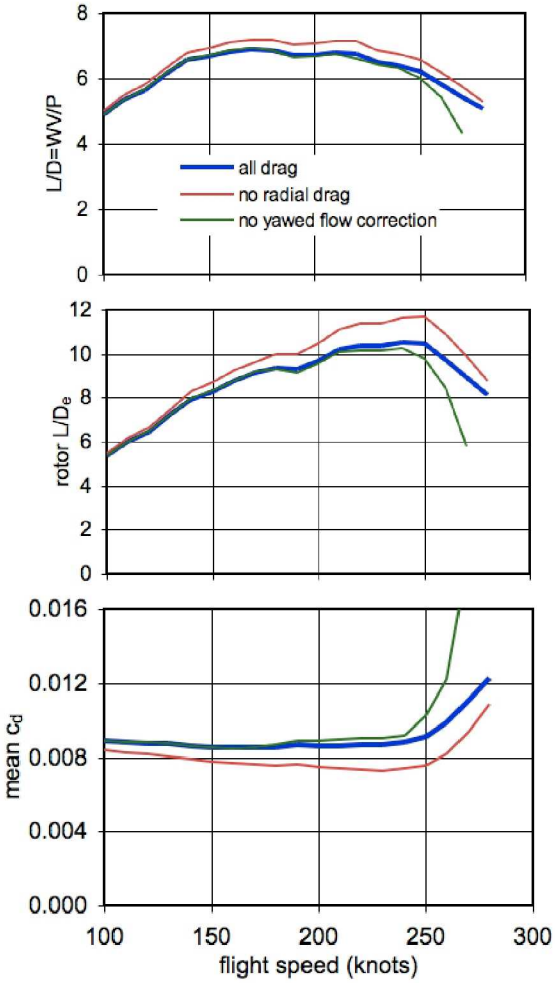


Figure 29. Influence of rotor-drag model on cruise performance.

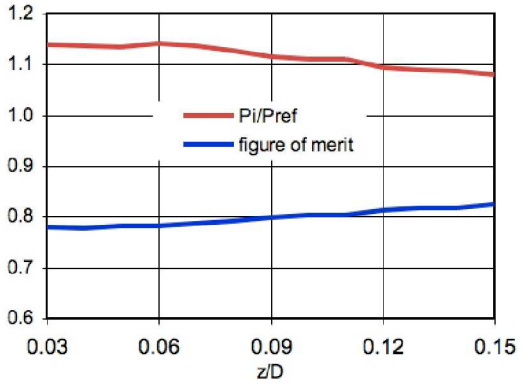


Figure 30. Hover performance for coaxial configuration, varying vertical separation.

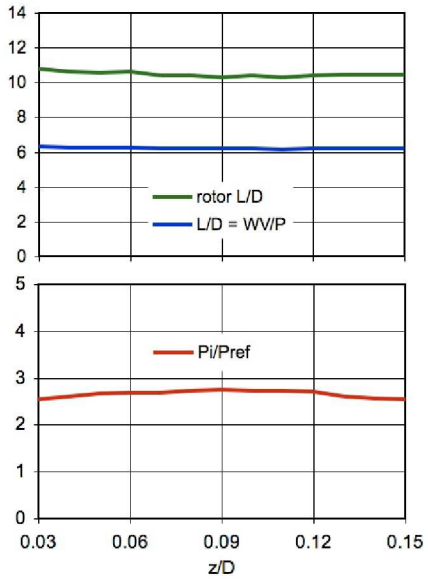


Figure 31. Cruise performance for coaxial configuration, varying vertical separation.

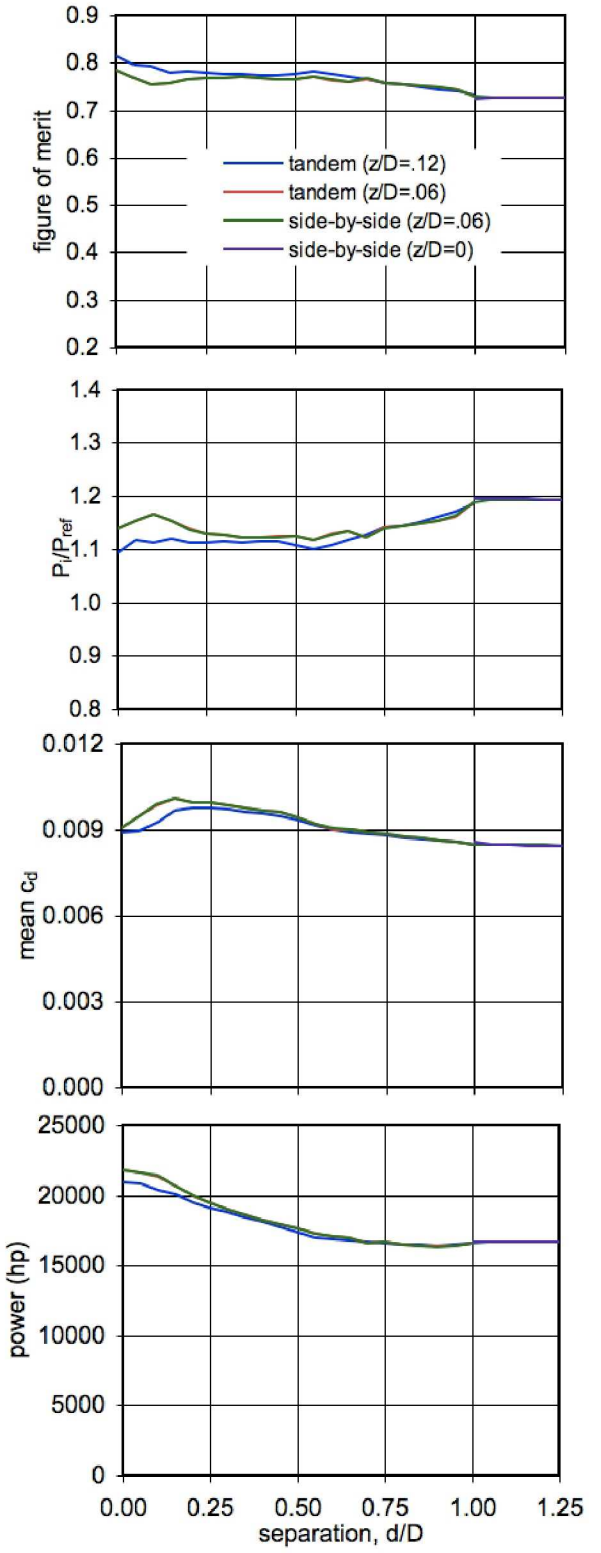


Figure 32. Hover performance for coaxial, tandem, and side-by-side configurations; constant rotor radius, varying rotor separation. Tandem and side-by-side at z/D = 0.06 identical; side-by-side at z/D = 0 only for d/D ≥ 1.

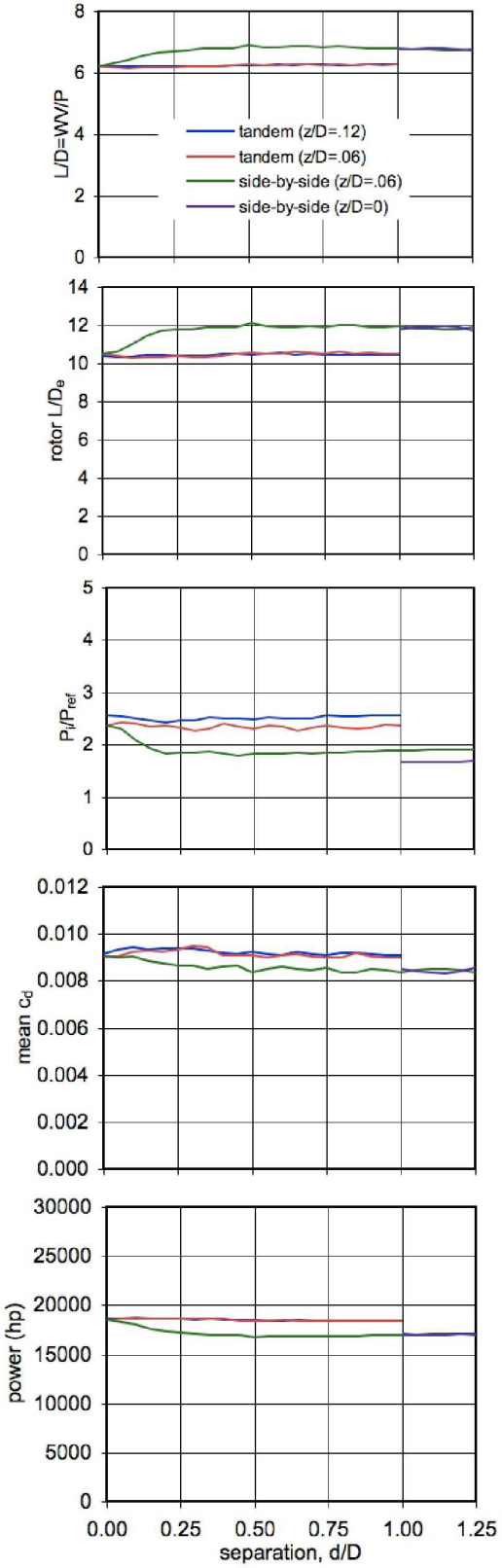


Figure 33. Cruise performance for coaxial, tandem, and side-by-side configurations; constant rotor radius, varying rotor separation.

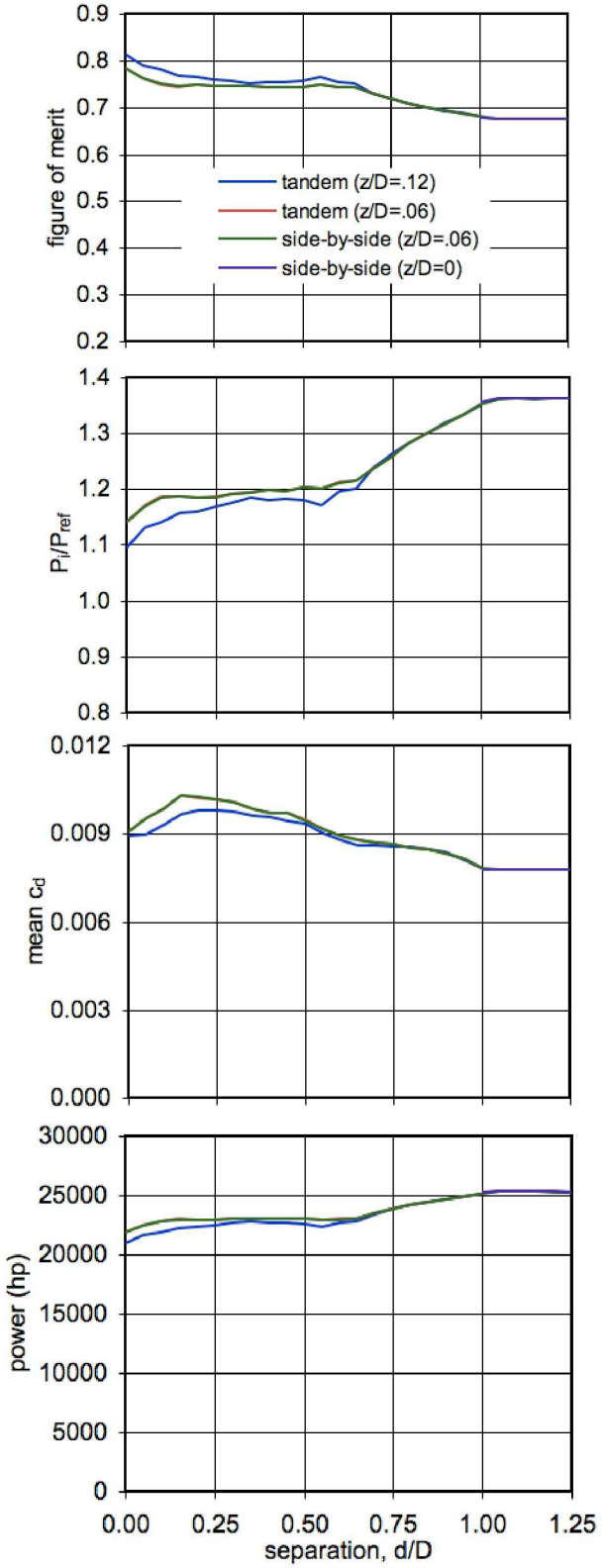


Figure 34. Hover performance for coaxial, tandem, and side-by-side configurations; constant disk loading, varying rotor separation. Tandem and side-by-side at z/D = 0.06 identical; side-by-side at z/D = 0 only for d/D ≥ 1.

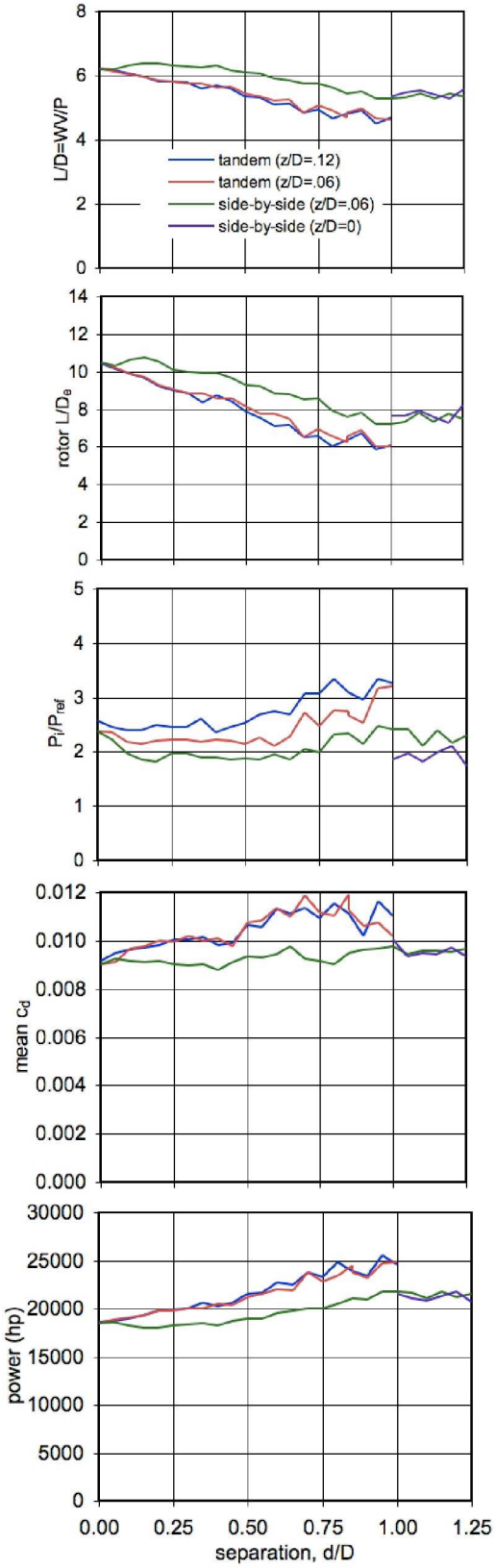


Figure 35. Cruise performance for coaxial, tandem, and side-by-side configurations; constant disk loading, varying rotor separation.

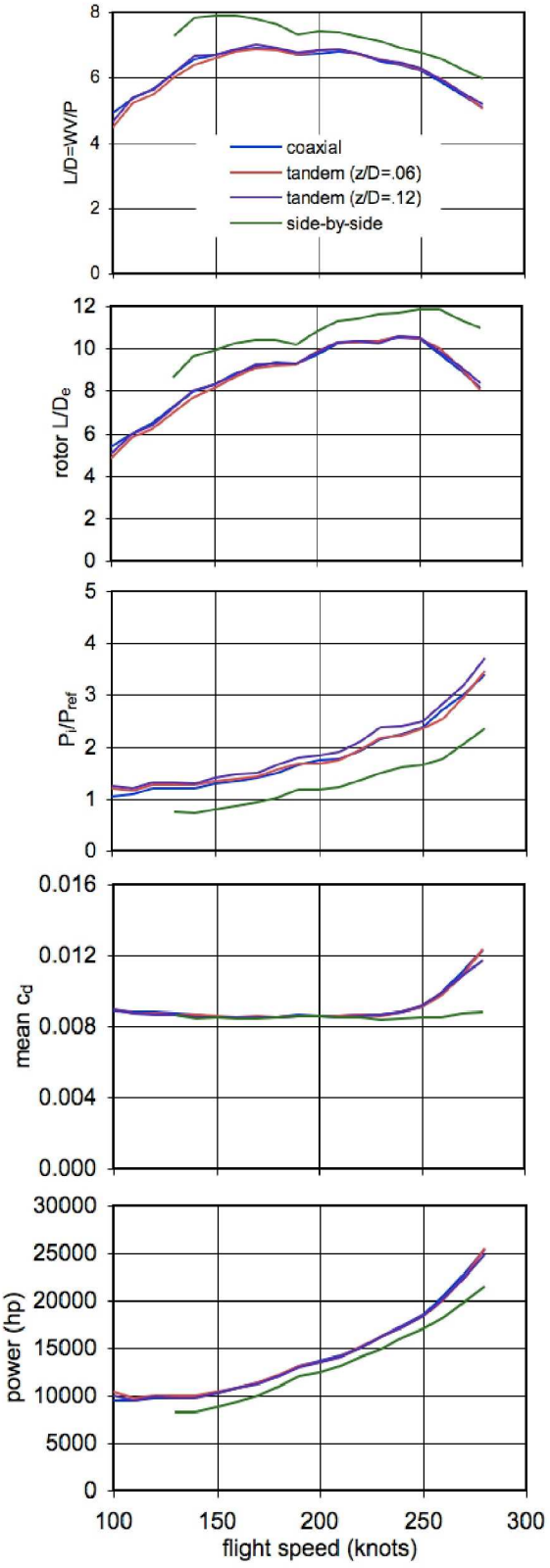


Figure 36. Cruise performance for coaxial, tandem, and side-by-side configurations; constant rotor radius.

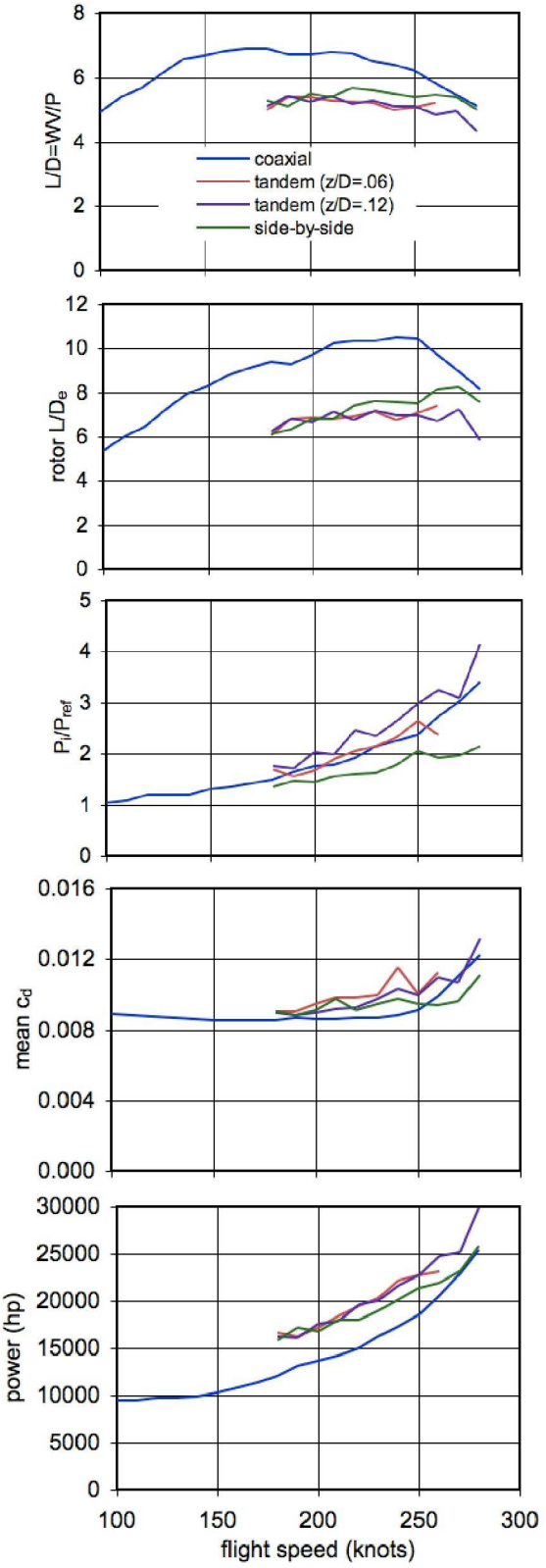


Figure 37. Cruise performance for coaxial, tandem, and side-by-side configurations; constant disk loading.

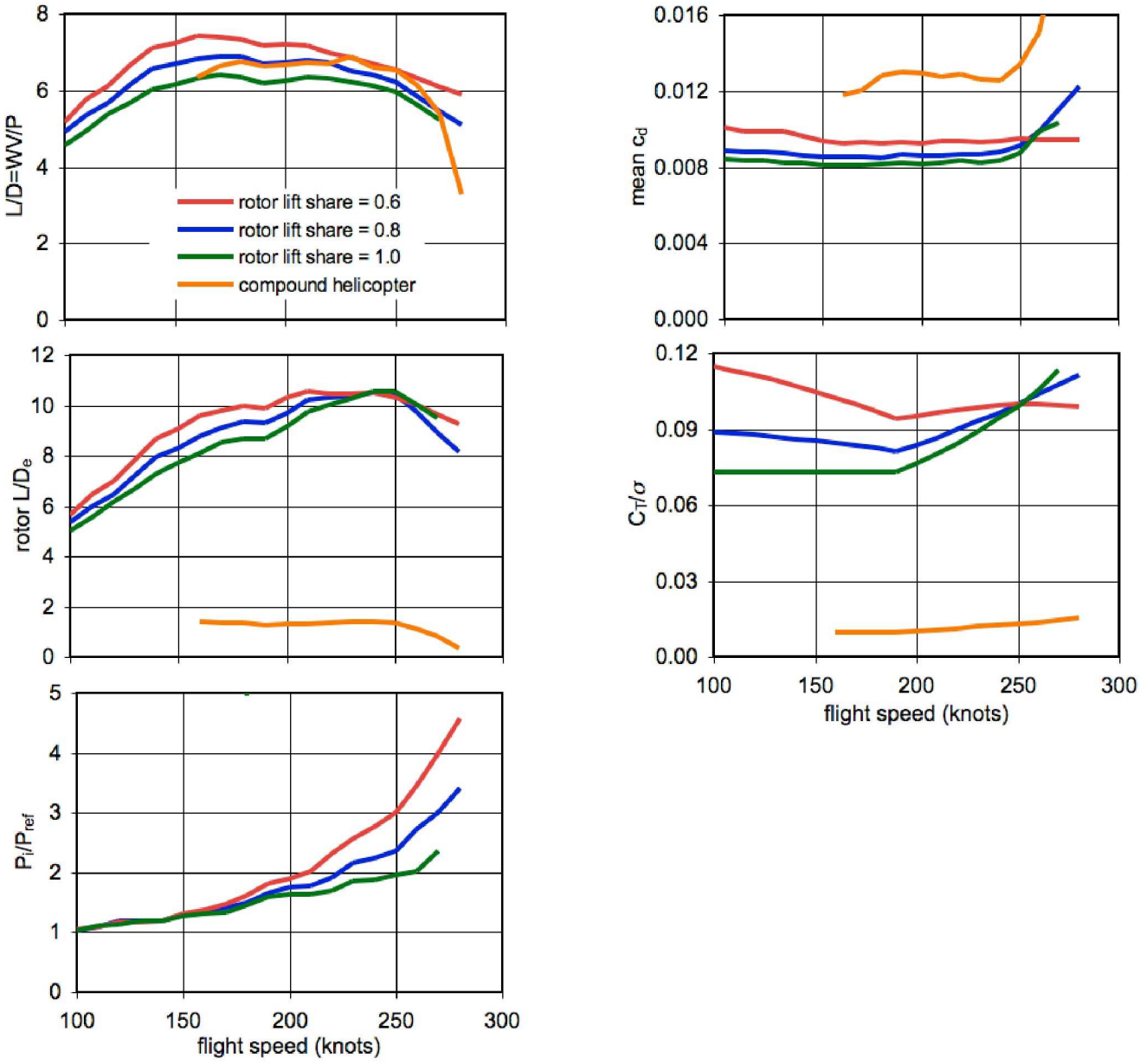


Figure 38. Influence of rotor lift share on cruise performance for coaxial configuration, including compound helicopter.